Lateral Membrane Heterogeneity Probed by FRET Spectroscopy and Microscopy

Luís M.S. Loura and Manuel Prieto

Abstract Förster resonance energy transfer (FRET) is a photophysical process highly dependent on interchromophore distance. Due to this feature, it is very sensitive to membrane lateral heterogeneity, as the donor and acceptor fluorophores involved in FRET tend to have different preference for distinct types of lipid bilayer domains. In this chapter, the basic formalisms of FRET in situations of increasing complexity (from a single donor-acceptor pair at a fixed distance to non-random probe distribution) are presented and illustrated with selected examples from the literature. The importance of time-resolved fluorescence data is emphasized. It is shown that FRET can be used to study the occurrence of domain formation, allowing their detection as well as size estimation. Lateral lipid distribution heterogeneity may also result from peptide- or protein-lipid interaction. Formalisms that apply to these situations are also presented, as well as selected examples of their use. Applications of FRET under the microscope have recently come to the fore, and representative studies are mentioned.

Keywords Energy Transfer · Fluorescence · Lipid Domains · Membrane Phase Separation · Rafts

L.M.S. Loura (✉)
Faculdade de Farmácia, Universidade de Coimbra, Pólo das Ciências da Saúde, Azinhaga de Santa Comba, 3000-548 Coimbra, Portugal

Centro de Química de Coimbra, Universidade de Coimbra, Rua Larga, 3004-535 Coimbra, Portugal
e-mail: lloura@ff.uc.pt

M. Prieto
Centro de Química-Física Molecular and Institute of Nanosciences and Nanotechnology, Complexo I, IST, UTL, Av. Rovisco Pais, 1049-001 Lisboa, Portugal

Y. Mély and G. Duportail (eds.), *Fluorescent Methods to Study Biological Membranes*, Springer Ser Fluoresc (2013) 13: 71–114, DOI 10.1007/4243_2012_59,
© Springer-Verlag Berlin Heidelberg 2012, Published online: 28 August 2012

Contents

1 Lipid Bilayer Phase Separation and Membrane Domains

The fluid mosaic model of biological membranes [122] emphasizes membrane fluidity and free lateral diffusion of membrane components. This led to the generalized idea of biomembranes as solutions of proteins embedded in bilayers of randomly distributed phospholipids. However, over the past few decades, it has become accepted in the field of membrane biophysics that lipid lateral heterogeneous distribution exists both in natural and model membranes. Because lipids in general do not mix ideally, the primary driving force for lipid phase separation stems from lipid-lipid interaction, although the presence of proteins can modulate this process, as commented below.

Lipid lateral phase separation was first detected and characterized in binary phospholipid lipid mixtures, in which the two components differed significantly in their main transition temperatures (T_m). This difference could be the result of a discrepancy in acyl chain length (e.g., 12:0,12:0 (*m*:*n* denotes a chain with *m* carbon atoms and *n* double bonds) phosphatidylcholine (PC)/18:0,18:0 PC; [85]), degree of unsaturation of the acyl chains (e.g., *trans*-Δ^9 18:1, *trans*-Δ^9 18:1 PC/18:0,18:0 PC; [146]) or headgroup structure (e.g., *trans*-Δ^9 18:1, *trans*-Δ^9 18:1 PC /16:0, 16:0 phosphatidylethanolamine (PE); [146]) of the two mixture components. The fact that phase separation occurs for mixtures of lipids coexisting in cell membranes under conditions close to physiological (e.g., [86]) made the detection and characterization of this kind of lateral heterogeneity of considerable interest in the biophysical and biochemical communities (e.g., [148]). The composition-temperature phase diagrams, derived under equilibrium conditions at constant pressure (and ionic strength, etc.), are a convenient way to represent this type of behavior for each pair of phospholipids. The classic book by Marsh [86] collects several of these examples, and a second, much expanded edition is expected around the time of publication of this work.

Another group of lipid mixtures that have been intensely used are phospholipid (mainly PC)/cholesterol (chol) binary systems. These mixtures' properties and interaction with peptides and proteins are of importance due to the high abundance of chol in mammalian plasma membranes. From the studies in model systems, important conclusions have been inferred about the role of sterols in biomembranes. The well-known effects of chol on the bilayer properties (see, e.g., [7, 96]) have been rationalized considering that in the presence of high amounts of chol in a PC

bilayer, the membrane is in a liquid ordered (lo) phase (using the nomenclature introduced by Ipsen et al. [58]), with intermediate properties between those of the gel and the fluid. This designation highlights the facts that the translational diffusion is closer to the fluid phase (the diffusion coefficient in the lo phase is only two to three times lower than for the pure fluid phase of the PC), but the acyl chains are in a much more ordered configuration. In this nomenclature, the gel and fluid phases are designated by solid ordered (so) and liquid disordered (ld), respectively. The phase diagram is monotectic, and for intermediate chol concentrations, phase coexistence occurs: so and lo, below the monotectic temperature (which is close to T_m), and ld with lo, above the monotectic temperature (a recent collection of these diagrams has been published; [87]). The latter corresponds to fluid-fluid phase separation, which is thought to be of biological relevance, namely, to the raft phenomenon (e.g., Brown and London [16]). These were at first operationally defined as insoluble membrane fractions upon detergent extraction (the so-called detergent resistant membranes, DRM), and their composition revealed that they were rich in chol, spingomyelin, and saturated lipids. Later, these membrane patches, which were intensively studied both in membrane biophysics and cell biology, were described as liquid-ordered on the framework of the above-mentioned type of phases postulated in the presence of chol. Although phase separation was not a novelty in itself, the very pictorial raft concept bridged the fields of membrane biophysics and cell biology, and the communication between these two communities was instrumental to develop a very active research on both natural membranes and their model systems.

It should be mentioned that for PC/chol systems, the most studied being 16:0,16:0 PC/chol, there are several phase diagrams reported that differ considerably (e.g., [72, 92, 140]). The discrepancies are probably related to the similarity between the two phases, which makes differentiation between them difficult [149]. Nevertheless, some of those discrepancies have been rationalized in a study of one of the archetypal raft model systems, the 16:0,18:1 PC/*N*-palmitoylsphingomyelin (PSM)/chol mixture [33]. Following this work, ternary lipid mixtures of high melting/low melting/chol (proposed as minimal model systems of raft-forming lipid mixtures) have been studied and described in terms of fixed-temperature, fixed pressure, ternary phase diagrams [52].

Several interconnected concepts can be misdealing, among them phases and membrane domains, and also the problem of their sizes. Phases and phase diagrams only apply to systems under thermodynamic equilibrium, and it should be stressed that this situation can be a very slow process. In a situation of very strong mismatch of two lipid components, i.e., when the driving force is very high, the time that it takes to attain equilibrium upon a system perturbation is on the scale of hours for gel-fluid phase separation [32, 63]. However, even considering that a cell membrane is not under equilibrium, phase diagrams are instrumental to the rationalization of the processes that can occur in a natural membrane. Also according to thermodynamic considerations, phase separation would proceed until completion in order to decrease line tension, so this would imply that the observed domains, whatever the methodology used, should be very large. This is observed for gel-fluid phase separation where the phase boundary is very steep, and defects are present.

However for liquid-ordered/liquid-disordered phase coexistence, the domains are small (submicron, "nanodomains"), as will be discussed later in detail in this chapter, and chol or specified lipid configurations have been invoked to be able to reduce line tension, thus preventing their growth [121]. It should be stressed that increasing the number of domains also leads to an entropic compensation.

The existing discussion in the literature about domain sizes was prompted by the different information obtained according to the different type of experimental approach used to detect and study them. While in natural membranes there is clear evidence that domains are in general small (10–100 nm, nanodomains) (see e.g., [59, 68, 90]), in model systems different answers were obtained depending on the methodology used. Under a confocal microscope, large (micron size) domains can be observed in suitable systems, namely, ternary systems with ld/lo phase separation, but up to now no phase separation was detected for binary systems with cholesterol [136]. This is in general attributed to the very small size of these lo domains, below the lateral resolution of the microscope (~300 nm), and it prompts a global discussion about the type of phase diagrams (and thus the phases and domain sizes) that are described in the literature. There is a clear disagreement when comparing the ones coming from microscopy data, with the ones obtained from spectroscopic approaches such as fluorescence and ESR as described by, e.g., Veatch and Keller [137]. From fluorescence spectroscopy, and in particular using FRET with adequate modeling, as described later in this chapter, clear evidence for nanoscopic domains is obtained and the same happens, e.g., from residence times data in the submicrosecond regime in ESR spectroscopy [22]. Therefore, more detail is obtained from spectroscopic approaches which do not miss the existence of small domains (and so phase separation). Along this way the use of "spectroscopic diagrams" was suggested [4]. Microscopy is however invaluable in the way that it allows direct visualization of lipid domains, and we can foresee in the future fast development in this area, such as near-field scanning optical microscopy (see [38] for a review), stimulated emission depletion microscopy, and related "super-resolution microscopy" approaches (see [102] for a review), which allow a closer-to-molecular resolution (~30 nm) as compared to standard confocal. Also, recently, in a powerful conjugation with AFM (e.g., [25]), this technique has been instrumental in the study of membrane domains.

Another subject under discussion is whether the nanodomains (assuming they are not transient density fluctuations) should be considered as phases, otherwise the phase diagrams based on their detection, as well as the respective tie-lines, would have no meaning. Apart from the problem that phase separation will not go up to completion as discussed before (but the same happens for the larger domains micron size domains detected by microscopy), there is no critical restriction on size that would prevent the phase concept of being applied to them. In addition, they are formed at least by a few thousand molecules, i.e., they are large enough for their rationalization as a phase in the framework of statistical thermodynamics. Another relevant aspect is that spectroscopic methodologies allow the derivation of phase diagrams that are thermodynamically consistent.

It should be mentioned that the structure and dynamics of biological membranes and their model systems constitute a very lively research area, and also the concept

of chol-induced lo and ld phases mentioned above has been questioned in recent literature using different approaches, e.g., X-ray diffraction [64] and NMR data [138]. However, in this chapter the discussion about phases and chol will be carried out in the framework of ld/lo phase separation, as this conceptualization proved to be instrumental in the rationalization of membrane biophysics.

Another source of lateral distribution heterogeneity is preferential interaction of proteins with selected lipids. These interactions are able to drive enrichment of the bilayer around the protein in these lipids and impoverishment in others, creating local heterogeneities that can potentially extend to several lipid shells around the protein. Some superficial membrane proteins demonstrate specific binding to some lipid classes, a phenomenon that can control protein recruitment to the membrane and activate signaling cascades [30]. In addition, transmembrane proteins display differential interactions with lipids of different acyl-chain lengths due to packing constraints in the lipid/protein hydrophobic interface, that have a significant effect on the activity of several proteins. Membrane proteins also have been shown to present binding sites for lipids in hydrophobic pockets away from the protein/lipid interface and binding of specific lipids to such sites is essential for activity in several cases [71]. In this chapter, we dedicate a subsection covering studies concerning protein-induced lipid heterogeneous distributions.

In all cases, we will focus on the application of Förster resonance energy transfer (FRET) to the systems at hand. For this purpose, it is useful to describe the basic formalisms of FRET and how they can be used in situations where molecule distribution is not uniform. This is done in the following section, which is organized in terms of increasing complexity (from the fixed donor-acceptor distance case to non-random fluorophore distribution formalisms, and from one-component, one-phase lipid bilayers to two- and three-component, phase-separated systems). Lipid distribution heterogeneity arising from protein-lipid interactions is described in a separate subsection. A brief finalizing section is dedicated to quantitative applications of FRET under the microscope to the study of heterogeneous lipid distribution in very large model systems (such as giant unilamellar vesicles (GUV)) and live cell membranes. As we focus on quantitative uses of FRET, phenomenological applications are not addressed in this chapter. On the other hand, unless explicitly mentioned otherwise, all formalisms and examples refer to the cases where donor and acceptor species are distinct species (hetero-FRET).

2 FRET Formalisms and Their Application in Spectroscopic Studies

2.1 One Donor – One Acceptor

FRET is a photophysical process by which an initially electronically excited fluorophore, termed “donor,” transfers its excitation energy (and thus becomes quenched) to another chromophore, termed “acceptor,” whose electronic

absorption spectrum overlaps that of the emission of the donor. The latter, initially in the electronic ground state, becomes excited upon transfer, and may (or may not) fluoresce. FRET involves neither photon emission nor molecular contact between the two species, but is highly dependent on the distance between them. For an isolated donor-acceptor pair, the (first-order) rate coefficient for the FRET interaction is proportional to the inverse sixth power of this distance [44]:

$$k_T = \frac{1}{\tau_0}\left(\frac{R_0}{R}\right)^6 \tag{1}$$

In this equation, τ_0 is the donor excited state lifetime in the absence of acceptor, R is the donor-acceptor distance, and R_0 is the so-called Förster radius. The latter is a characteristic length for FRET, defined as the donor/acceptor distance for which FRET within a given donor/acceptor pair is 50 % efficient (i.e., as probable as the other processes of donor excitation decay). In practice, the distance range for which FRET is sensitive is between 0.5 R_0 and 2 R_0, as FRET efficiency varies from 98.5 % to 1.5 % in this interval. The value of R_0 is characteristic of each donor/acceptor pair in a given environment, but usually lies in the 1.5–6 nm range. It can be calculated from spectral data using the following equation:

$$R_0 = 0.2108\left[\kappa^2 \cdot \Phi_D \cdot n^{-4} \cdot \int_0^\infty I(\lambda) \cdot \varepsilon(\lambda) \cdot \lambda^4 d\lambda\right]^{1/6} \tag{2}$$

where κ^2 is the FRET orientation factor (for a definition and discussion of κ^2, see [134]), Φ_D is the donor fluorescence quantum yield, n is the medium refractive index, $I(\lambda)$ is the donor normalized emission spectrum, and $\varepsilon(\lambda)$ is the acceptor absorption spectrum.

A convenient metric of the extent of FRET is the FRET efficiency, E, defined as the ratio between the rate of FRET and that of donor decay considering all pathways:

$$E = k_T \Big/ \sum_i k_i = k_T \tau \tag{3}$$

where τ is the donor lifetime in the presence of acceptor. For an experimental situation where all donor/acceptor pairs are identical and fluorophore diffusion can be neglected during the donor excited state lifetime (so that R has a fixed determined value),

$$E = 1 - \tau/\tau_0 = R_0^6/(R^6 + R_0^6) \tag{4}$$

An identical expression can be written for the fluorescence quantum yield. By rearranging this equation, one obtains R:

$$R = R_0 \left(\frac{1 - E}{E} \right)^{1/6} \tag{5}$$

These equations explain the use of FRET as a "spectroscopic ruler" [128], as it allows the measurement of distances of the order of R_0 from knowledge of the latter and measurement of E. As mentioned above, they apply strictly to a situation where all donor/acceptor pairs have identical separating distance. In case of conformational flexibility, modifications can be introduced that allow recovery of distance distributions or characterization of diffusion in a linked donor/acceptor pair (e.g., [70], and references therein). Additionally, expressions that relate the efficiency of FRET to geometrical parameters in a cluster of a finite number of donors and/or acceptors can be derived by taking into account the multiple FRET rate terms (Eq. 1) in the calculation of the overall FRET efficiency (which may be relevant to characterize oligomerization, e.g., [73]). However, it must be stressed that the most common situation in membranes is that of donor and acceptor fluorophores scattered in a quasi-two-dimensional geometrical arrangement, leading to a multitude of undetermined donor/acceptor separation distances. Even though for each particular pair Eq. 1 is still valid, the overall complexity rules out the use of Eq. 5 for distance determination (a distance retrieved from Eq. 5 would be a very complex average from which no useful information can be recovered). These scenarios require modeling using formalisms for infinite planar or bilayer geometry, as outlined in the following section.

2.2 *One Donor – Multiple Acceptors in Bidimensional Media*

2.2.1 Uniform Probe Distribution

We now move to the situation where all donors and acceptors are scattered in a plane and each donor fluorophore is surrounded by a uniform distribution of acceptors. We will assume for now that all donors are equivalent (so that one needs only to consider one donor molecule), no lateral diffusion is operative during the donor lifetime, and all donor/acceptor pairs have the same R_0 value. From Eq. 1, the total rate of FRET from the donor molecule under consideration to the N acceptor molecules located inside a disk of radius R_d (and centered on this particular donor) is

$$k_T = \tau_0^{-1} \left[1 + \sum_{i=1}^{N} (R_0/R_i)^6 \right] \tag{6}$$

where R_i is the distance between the donor and the i-th acceptor inside the disk. As shown previously [46, 145], this approach leads to closed-form analytical solutions. If the minimum donor-acceptor distance R_e (also termed "exclusion distance") is

much smaller than R_0 (in practice, if $R_e < R_0/4$), the time evolution of donor fluorescence in presence of acceptor (i_{DA}) is simply given by

$$i_{DA}(t) = \exp(-t/\tau_0)\exp\left[-\pi\Gamma(2/3)R_0^2 c(t/\tau_0)^{1/3}\right] \tag{7}$$

In this equation, Γ is the complete gamma function and $c = N/(\pi {R_d}^2)$ is the average number of acceptors per unit area. In case that R_e and R_0 are of the same order, the donor decay becomes more complex [145]:

$$i_{DA}(t) = \exp\left(-\frac{t}{\tau_0}\right)\exp\left\{-\pi R_0^2 c\gamma\left[\frac{2}{3}, \left(\frac{R_0}{R_e}\right)^6\left(\frac{t}{\tau_0}\right)\right]\left(\frac{t}{\tau_0}\right)^{1/3}\right\}\cdot$$
$$\cdot\exp\left\{\pi R_e^2 c\left(1-\exp\left[-\left(\frac{R_0}{R_e}\right)^6\left(\frac{t}{\tau_0}\right)\right]\right)\right\} \tag{8}$$

Here γ is now the incomplete gamma function. Equation 8 also applies to the situation where the planes of donors and acceptors are distinct but parallel, separated by a transverse distance w [145]. This condition is often met in membrane studies, as donor and acceptor depths of location in the bilayer are frequently distinct. In this case, $R_e = ({R_l}^2 + w^2)^{1/2}$, where R_l is the minimum donor-acceptor lateral distance (i.e., parallel to the membrane plane).

Depending on the experimental setup, acceptors may locate in two parallel planes rather than in a single plane. This is expected if, for example, they are evenly distributed between the two bilayer leaflets. In this case, there will be two R_e distances, one for each plane of acceptors. Computation of i_{DA} from Eq. 8 requires multiplying by two additional exponential terms, identical to the last two of the right-hand side, differing only in the value of R_e.

If the FRET measurement is carried out under photostationary conditions, the decay is not measured, and it is convenient to compare the experimental value of FRET efficiency (Eq. 4) with that expected from the above formalism. The latter can be computed from numerical integration:

$$E = 1 - \int_0^\infty i_{DA}(t)dt \Big/ \int_0^\infty i_D(t)dt \tag{9}$$

Here i_D (equal to $\exp(-t/\tau_0)$ for an exponentially decaying donor) is the time-resolved donor fluorescence in the absence of acceptor.

The formalism of two-dimensional FRET was first applied to bilayer systems (unilamellar vesicles of egg yolk PC) in the pioneering study of Fung and Stryer [46]. Four donor/acceptor pairs (using dansyl- and eosin-head-labeled phosphatidylethanolamine derivatives), with spectroscopic R_0 values ranging from 2.3 to 5.1 nm, were considered. The authors analyzed steady-state FRET efficiencies with a formalism

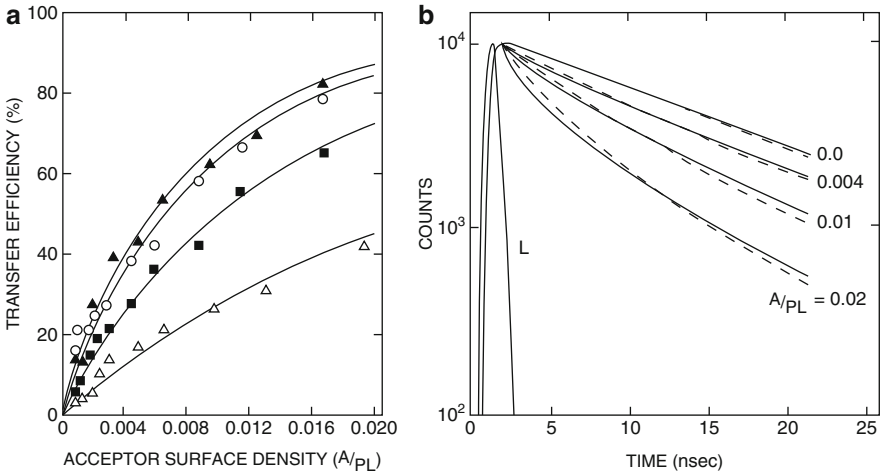

Fig. 1 (**a**) FRET efficiency as a function of the surface density of energy acceptor (acceptors per phospholipid) for four donor-acceptor pairs in egg yolk PC vesicles: *N*-(2-dimethylaminonaphthalene-6-sulfonyl)phosphatidylethanolamine (2,6-DPE) to *N*-(2-dimethylaminonaphthalene-5-sulfonyl)phosphatidylethanolamine (2,5-DPE) (*open triangles*); 2,6-DPE to *N*-eosin-*N*'-phosphatidylethanolaminothioureia (EPE) (*filled squares*); *N*-(l-dimethylaminonaphthalene-5-suIfonyl)phosphatidylethanolamine (1,5-DPE) to EPE (*open circles*); and 2,5-DPE to EPE (*filled triangles*). The lines are best-fit curves using the model of uniform probe distribution with R_0 values of 25.5, 37.5, 49, and 46 Å, respectively (compared with the values calculated from spectral data, 22.8, 39.1, 51.2, and 48.7 Å, respectively). (**b**) Fluorescence emission kinetics of 2,6-DPE in PC vesicles containing 0,0.004,0.01, and 0.02 molecules of EPE per molecule of PC (*dashed lines*). Synchrotron radiation was used as a pulsed light source (λexc = 350 nm, emission was viewed through a 440-nm interference filter). The decay curves were calculated using $R_0 = 39.5$ Å. $R_e = 8.4$ Å and $\tau_0 = 13.2$ ns, and then convoluted with the light pulse (*solid lines*) (Reprinted from Fung and Stryer [46] with permission. Copyright 1978 American Chemical Society)

equivalent to the combination of Eqs. 8 and 9 above, using R_0 as the sole optimized parameter. The recovered and calculated R_0 values differed less than 0.3 nm in all cases (Fig. 1a). The authors also measured donor fluorescence decays in the presence of varying concentration of acceptor for one of the studied FRET pairs. They verified that even though there was excellent agreement between the experimental decays and the theoretical expectations for low acceptor concentrations, deviations become apparent for higher acceptor loads (Fig. 1b). The observation of slower decays than predicted at short times was interpreted by the authors as possibly reflecting fewer short-distance donor-acceptor pairs than statistically expected, owing to both donor and acceptor probes being negatively charged. This shows that, right from the very first FRET application to bilayer systems, several important features were revealed: first, FRET in fluid bilayers was overall well described by the analytical two-dimensional formalism; second, deviations can be interpreted in terms of non-homogeneous fluorophore distribution; third, these deviations are much more evident in time-resolved experiments compared to steady-state conditions. The authors

rightly predicted that FRET would become a most valuable tool for the study of phenomena including lipid phase separation and protein oligomerization.

Following this study, it took some time for quantitative applications of FRET (rather than phenomenological studies, which are not considered here) to membrane heterogeneity to fully blossom. This can be understood by noting that laboratories equipped with laser excitation sources, capable of adequate time resolution, were relatively scarce during much of the 1980s and even the 1990s, and analysis of time-resolved FRET data with formalisms such as described above was overwhelmingly slow before the development of affordable modern computers. At first, following Fung and Stryer's study, applications of the uniform distribution formalism to one-component bilayers aimed at verifying the applicability of Förster FRET theory to model membranes using different FRET pairs. From time-resolved data of FRET from *N*-(7-nitrobenz-2-oxa-1,3-diazol-4-yl) (NBD)-16:0,16:0 PE to *N*-(lissamine–rhodamine B) (Rh)-16:0,16:0 PE in 18:1,18:1 PC [69], a linear variation of the recovered c parameter as a function of the acceptor concentration was verified, as expected, allowing the calculation of the area per lipid molecule. This dependence was also verified in FRET from octadecylrhodamine B (ORB) to 1,1′,3,3,3′,3′-hexamethylindotricarbocyanine [$DiIC_1(7)$] in fluid 16:0,16:0 PC large unilamellar vesicles (LUV) [76]. In this study, a modified Eq. 7 was derived for biexponentially decaying donors, and the decays were globally analyzed, with linkage of donor lifetimes and preexponential ratio. However, analysis of the decays for the same system but below the main transition temperature was not successful, pointing to probe aggregation in the gel phase, possibly in line defects in the gel-phase structure. In this situation, the traditional framework, derived assuming a random distribution of probes, is no longer valid. This situation was also verified for the *N*-NBD-16:0,16:0 PE/*N*-Rh-16:0,16:0 PE pair in the same system [77]. In the latter study, a generalized FRET model, assuming distribution of acceptor concentrations [74], was also applied.

Presently, the uniform distribution formalism is still used as a test of whether addition of a new component to a given one-phase lipid bilayer system induces compartmentalization and/or phase separation. This would be detected in the failure to analyze FRET kinetics with uniform probe distribution formalisms. Recent examples of this kind include a study that demonstrated the absence of clustering of phosphatidylinositol-(4,5)-bisphosphate ($PI(4,5)P_2$) in a fluid PC matrix at slightly above physiological pH, following the satisfactory description of FRET between 1,6-diphenylhexatriene (DPH) and NBD-labeled $PI(4,5)P_2$, in 16:0, 18:1 PC vesicles with 5 mol% of total $PI(4,5)P_2$ [43] at pH 8.4. On the other hand, time-resolved FRET between the tryptophan residues of acetyl-$GWW(LA)_8LWWA$-amide peptide (WALP23) to the fluorescent chol analog dehydroergosterol (DHE), both with and without added equimolar amounts of chol, could be satisfactorily globally analyzed assuming uniform DHE distribution in the bilayer [51]. This FRET pair (tryptophan/DHE) was also used in a study of the hypothetical affinity of the γM4 peptide from the muscle acetylcholine receptor (donor: Trp453) for chol (acceptor: DHE) in the lo phase of 16:0, 18:1 PC/Chol. The measured FRET efficiencies were significantly lower than expected, which was interpreted on the basis of formation of peptide-rich, sterol-depleted patches [34]. Higher FRET efficiency than expected was observed

between M13 major coat protein labeled with *N*-(iodoacetyl)aminoethyl-1-sulfonaphthylamine (IAEDANS, donor) and *N*-(4,4-difluoro-5,7-dimethyl-4-bora-3a,4a-diaza-s-indacene-3-yl)methyl iodoacetamide (BODIPY, acceptor) in supposedly monophasic (fluid) bilayers of *cis*-Δ^{13} 22:1, *cis*-Δ^{13} 22:1 PC/18:1, 18:1 PC and *cis*-Δ^{9} 14:1, *cis*-Δ^{9} 14:1 PC/18:1, 18:1 PC, due to formation of domains enriched in the protein and the matching lipid (18:1, 18:1 PC; [41]).

Sometimes addition of a component leads to changes in FRET efficiency that are not related to phase separation, but to other morphological changes in the lipid organization. This was the case in recent studies of mixed PC/anionic lipid (phosphatidylserine, PS) vesicles incubated with a basic peptide (K_6W; [80]) or protein (lysozyme; [27]), where formation of stacked lipid multilayers, bridged by peptide or protein, was concluded. Whereas the observed FRET efficiency variations could be due to either lateral demixing or multilayer formation, global analysis of time-resolved data can clearly distinguish between the two situations. In the mentioned studies, no significant lateral phase separation takes place. The variations in the extent of FRET result from multilayer formation, and it was even possible to measure the spacing repeat distance in these structures.

2.2.2 Phase Separation into Large Domains

Although the above equations refer to uniform fluorophore distribution, the generalization to a biphasic environment is straightforward, provided that the two phases involved are organized in large domains on the FRET length scale (i.e., much larger than R_0). The key idea is that in such a situation there are two donor and two acceptor populations, each characteristic of one of the coexisting phases. Probe concentrations are different in the two phases, but it is assumed that distribution remains uniform within each type of domains. Additionally, the hypothesis of large domains implies that boundary effects are negligible, that is, donors located in one phase only sense acceptors located in the same phase, and interphasic FRET may be ignored. With these assumptions, the donor decay in presence of acceptor is a linear combination of the donor decays $i_{DA,i}$ inside the coexisting phases (labeled $i = 1, 2$):

$$i_{DA}(t) = A_1 i_{DA,1}(t) + A_2 i_{DA,2}(t) \tag{10}$$

In this equation, the coefficients A_i are proportional to the amount of donor in the corresponding phase (provided that molar absorptivity is the same in the two phases), and $i_{DA,i}$ is given by Eq. 7 or 8 above. For each phase, characteristic values of τ_0, c, R_0, and possibly R_e apply. Considering this, it follows that the total number of parameters in Eq. 10 is very large, and donor decays in presence of acceptor are best analyzed simultaneously with linked values of common parameters (global analysis) with decays in absence of acceptor for a more accurate retrieval of the best fitting parameter values. The latter contain information relative to the amount of

donor and acceptor in each phase, from which the partition coefficients of these probes may be calculated. These are defined as (e.g., [31]):

$$K_p = (P_2/X_2)/(P_1/X_1) \tag{11}$$

where P_1 is the probe mole fraction in lipid phase 1, and X_1 is the lipid phase 1 mole fraction (therefore $P_2 = 1 - P_1$ and $X_2 = 1 - X_1$). The partition coefficients of donor (K_{pD}) and acceptor (K_{pA}) probes can be calculated straightforwardly from the FRET decay parameters [78],

$$K_{pD} = (A_2/X_2)/(A_1/X_1) \tag{12}$$

$$K_{pA} = (c_2 a_2/\tau_2^{1/3}) \Big/ (c_1 a_1/\tau_1^{1/3}) \tag{13}$$

where a_i is the area per lipid molecule in phase i. These equations were originally applied to a situation of gel/fluid phase separation in the aforementioned 12:0,12:0 PC/18:0,18:0 PC system. Two different temperatures and compositions inside the phase coexistence range were studied. The short-tailed FRET donor, *N*-NBD-12:0,12:0 PE, and a short-tailed FRET acceptor, 1,1′-didodecil-3,3,3′,3′′-tetramethylindocarbocyanine ($DiIC_{12}(3)$), were shown to prefer the fluid phase (rich in short-tailed phospholipid) by both intrinsic anisotropy, lifetime and FRET measurements, in agreement with published reports. The other studied FRET acceptor, long-tailed probe 1,1′-dioctadecil-3,3,3′,3′-tetramethylindocarbocyanine ($DiIC_{18}(3)$), was expected to prefer the gel (rich in long-tailed phospholipid), on account of hydrophobic matching considerations [95]. While intrinsic lifetime studies indeed indicated preferential partition of $DiIC_{18}(3)$ into a rigidified environment, FRET analysis pointed to an increased donor-acceptor proximity as a consequence of phase separation. These apparently conflicting results were rationalized on the basis of segregation of $DiIC_{18}(3)$ to the gel/fluid interphase. In order for fluid-located donors to sense these interphase-located acceptors, fluid domains should be small (not exceeding ~10–15 nm). This work shows that membrane probes which apparently prefer the gel phase may show a nonrandom distribution in this medium (in agreement with the study described above for pure DPPC gel phase LUV) and tend to locate in an environment which simultaneously leads to less strict packing constraints and to favorable hydrophobic matching interactions.

The dynamics of domain growth was also studied in the 12:0,12:0 PC/18:0,18:0 PC (equimolar composition) [32]. LUV were first equilibrated at 65 °C, a temperature above the T_m of both lipids, where the system is in the one fluid (supposedly homogeneous) phase situation. The lipid vesicles contain also a probe that partitions preferentially to the gel (*trans*-parinaric acid, *t*-PnA) and another that prefers the fluid phase (*N*-NBD-12:0,12:0 PE). Then, a sudden thermal quench to 20 °C is carried out, and the lipid mixture is rapidly taken to the gel/fluid phase coexistence region of the phase diagram (Fig. 2a). The FRET efficiency as a function of time was measured and, as expected, it decreased, because as domains

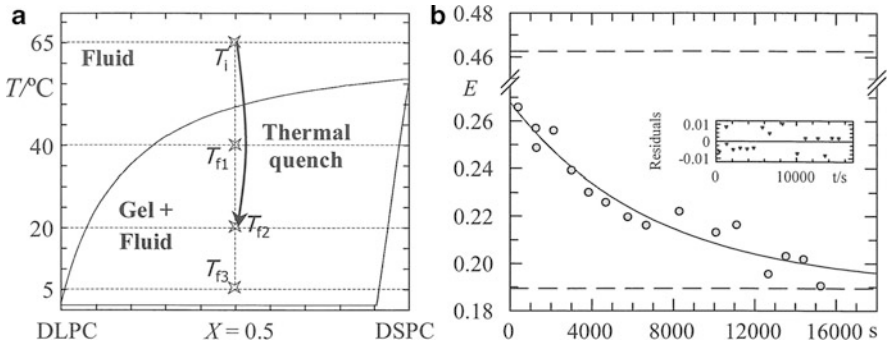

Fig. 2 (**a**) Phase diagram 12:0,12:0 PC/18:0,18:0 PC (adapted from [3]). The initial temperature (T_i) and the three final temperatures (T_f) after the thermal quenches are shown. (**b**) FRET efficiency E from *t*-PnA to *N*-NBD-12:0,12:0 PE vs. time equimolar 12:0,12:0 PC/18:0,18:0 PC LUV after a sudden thermal quench from $T_i = 65$ °C (fluid phase region) to $T_f = 20$ °C in the gel/fluid coexistence region. The line is the best fit of an exponential function with a nonzero infinite value, and the residuals are shown in the insert. The two limiting E values were calculated assuming uniform distribution of both probes at zero-time (*dashed line* above in the plot) and complete phase separation at infinite time (*dashed line* below in the plot), respectively (Reprinted from de Almeida et al. [32] with permission. Copyright 2002 Biophysical Society)

form and grow due to the differential portioning of the probes, the donor is sensing a decreasing local concentration of acceptors. The process has a dynamics on the time-scale of hours. The trend of FRET efficiency with time could be well described by an exponential function with a nonzero value at infinite time ($E = 0.19$), equal to the calculated value considering infinite phase separation (Fig. 2b). This shows that domains are at least 5–10 times R_0 [79], in apparent contradiction with the study described above with $DiIC_{18}(3)$ as acceptor. These two sets of results can be reconciled by assuming that $DiIC_{18}(3)$, by probably accumulating in the gel/fluid interface, lowers the line tension of the interface separating the two coexisting phases, promoting bilayer reorganization into smaller domains. This effect would not occur with *t*-PnA, which is able to accommodate its single chain in the bulk gel.

Besides probe partition, the composition/temperature (x, T) phase diagram boundaries (x_1 and x_2, corresponding to pure 1 and 2 phases, respectively) may also be obtained from the time-resolved FRET parameters [79]. To show this, we let F be the overall acceptor mole fraction and F_i be the acceptor mole fraction within phase i. The latter is related to c_i according to

$$F_i = c_i a_i \tag{14}$$

By inserting the F_i values into the acceptor mass balance equation,

$$F = F_2(1 - X_1) + F_1 X_1 \tag{15}$$

X_1 and X_2 can be straightforwardly calculated, even for an unknown phase diagram. If this is carried out for two points, A(x_A, T) and B(x_B, T), and combined

with the lever rule, one obtains the following simple expressions for the phase boundaries:

$$x_1 = (x_A X_{2B} - x_B X_{2A})/(X_{1A} - X_{1B}) \quad (16)$$

$$x_2 = (x_B X_{1A} - x_A X_{1B})/(X_{1A} - X_{1B}) \quad (17)$$

If this procedure is repeated for several temperatures, the phase diagram is obtained.

More recently, Buboltz [17] developed an experimental approach (Steady-State Probe-Partitioning FRET or SP-FRET) for characterization of phase separation in lipid membranes, based on acceptor steady-state sensitized emission, and assuming that the coexisting phases are much larger than R_0. The procedure requires measurements with different FRET pairs exhibiting complementary partitioning. Sensitized emissions in each phase are expressed as a function of local donor and acceptor mole fractions, and two constants including all photophysical effects in the respective phase. On the low acceptor concentration regime, this relationship was significantly simplified [18]. Information on the phase boundaries can be obtained from the detection of the lipid compositions for which the gradient of sensitized acceptor emission relative to composition was maximal. In turn, model fitting to the sensitized fluorescence data, together with knowledge of the phase boundaries of the lipid system under study, allows for determination of the probes' interphasic partition coefficients as the sole fitting parameters. The author successfully applied this approach to the study of gel/fluid phase separation in 12:0,12:0 PC/18:0,18:0 PC mixtures by globally fitting data obtained from two different combinations of donor/acceptor pairs. The need for multiple donor/acceptor pairs is a consequence of the degeneracy of the model with respect to the partition coefficients of the probes in each set of measurements.

In another study, the same methodology for detection of phase boundaries was used for the characterization of the 18:1,18:1 PC/16:0,16:0 PC/chol lipid mixture [19]. Fluorescence data from 1294 independently prepared samples were analyzed and phase boundaries were obtained from the gradients of acceptor sensitized emission from 3,3′-dioctadecyloxacarbocyanine (18:0-DiO), using DHE as the FRET donor (Fig. 3). Three different regions of phase coexistence were clearly identified (gel/fluid, lo/ld, and lo/Chol crystals), presenting some discrepancies relative to confocal fluorescence microscopy (CFM) and solid-state NMR studies [136, 139]. Notably, the lo/ld coexistence range is narrower at room temperature (not extending beyond 33 mol% Chol, compared to 50 mol% for the CFM boundary). Also, as the temperature increases, coexistence in that region extends in its entirety to higher 16:0, 16:0 PC content, whereas for CFM measurements only the ld boundary is affected. The authors attribute this discrepancy to the use of different methodologies in sample preparation. CFM and solid-state NMR require film deposition of lipid to produce GUV or oriented membranes, and this might result in increased susceptibility to demixing of lipid components, while in this study, polydisperse multilamellar vesicle suspensions were prepared through the rapid

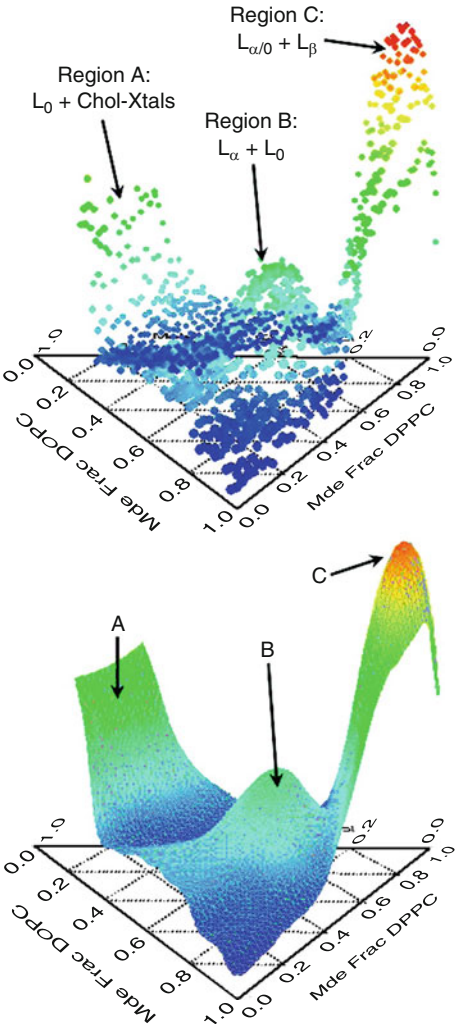

Fig. 3 Derivation of the phase boundaries of the 18:1,18:1 PC/16:0,16:0 PC/chol phase diagram using SP-FRET. Changes in sensitized acceptor fluorescence are plotted versus lipid composition in triangular coordinates. In the scatter plot on top, each data point corresponds to an independently prepared sample (1,294 total). The bottom plot shows a smooth surface fit to the same data (Reprinted from Buboltz et al. [19]. Copyright 2007 American Chemical Society)

solvent exchange method, which does not require formation of this intermediate lipid film. Interestingly, two other studies on this ternary system were recently published, neither of which restricted to GUV. De Almeida et al. [36], using a combined time-resolved fluorescence microspectroscopic approach (i.e., fluorescence lifetime imaging microscopy and microscopic fluorescence decays measured in GUV, and macroscopic fluorescence decays measured in large unilamellar vesicles), established the existence of the three-phase triangle near the 16:0/16:0 PC corner, thus narrowing the lo/ld range previously reported [139]. In the same year, an NMR study of multilamellar vesicles by Veatch and coworkers [138] indicated that lo/ld coexistence region does not extend beyond 35 mol% chol for 10–37 °C. SP-FRET was also the basic tool used recently in the study of 18:0,18:0

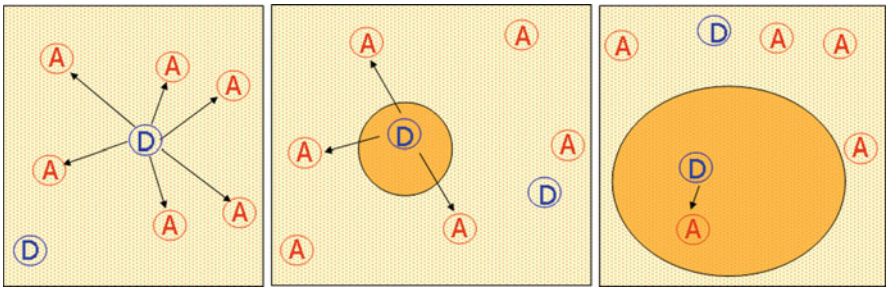

Fig. 4 Pictorial view of FRET between donor and acceptor preferring different phases in situation of: *left panel* – no phase separation (random distribution); *middle panel* – phase separation with small domains; *right panel* – phase separation with large domains (infinite phase separation limit) (Reprinted from de Almeida et al. [37] with permission. Copyright 2009 Elsevier)

PC/16:0,18:1 PC/chol and 18:0,18:0 PC/18:0,18:1 PC/chol, revealing the existence of small liquid domains, not observable by optical microscopy [48].

2.2.3 The Intermediate Case: Nanometer-Sized Domains

Many spectroscopic and other (calorimetry, X-ray diffraction) techniques have been informative in the identification of the phases present in a lipid mixture and in the derivation of phase diagrams (e.g., [52, 87]), and certainly are better suited than FRET to this purpose. On the other hand, it is certainly more convenient to use the variation of fluorescence parameters such as steady-state intensity, anisotropy, or lifetime to characterize the partition of membrane probes and fluorophore-bearing biomolecules, rather than to estimate them from the FRET decay fitting parameters. The major advantage of FRET is that its distance dependence, as expressed in Eq. 1, warrants a unique sensitivity to compartmentalization in its characteristic length scale, that is, of the order of R_0. Concerning membrane organization in particular, this feature allows FRET to report on formation of nanometer-sized domains, smaller than the limit of conventional optical microscopy. Consider the case of probes with complementary phase preference (Fig. 4). Phase separation will increase donor-acceptor separation and hence render FRET less efficient. However, if the domains formed are of the order of R_0, FRET between donors and acceptors located in distinct phases is significant, and FRET efficiency will fall between the values expected for the single-phase and two-infinite-phases scenarios. However, the obvious loss of symmetry and topological complexity of this intermediate regime has precluded the derivation of an exact solution of the FRET equations that allows convenient retrieval of the domain size for a given system. Several more or less approximate methodologies have been developed since the last decade to estimate domain sizes, which are succinctly described below.

Loura et al. [79] applied the infinite phase separation formalism described in the previous section to FRET between *N*-NBD-14:0, 14:0 PE (donor) and *N*-Rh-14:0,

14:0 PE (acceptor) dispersed in mixed 14:0, 14:0 PC/chol vesicles. The phase diagram for this system was known from discontinuities in electron spin resonance spectroscopy experiments and breaks in the behavior of the diffusion coefficient as determined from fluorescence recovery after photobleaching [3]. Six temperature/composition points were explored inside the lo/ld phase coexistence region: chol mole fraction $x_{chol} = 0.15$, 0.20, and 0.25, at temperatures $T = 30$ °C and 40 °C. The partition coefficients of the probes were determined from variation of steady-state intensity (*N*-Rh-14:0, 14:0 PE) or anisotropy (*N*-NBD-14:0,14:0 PE), revealing complementary phase preference (*N*-NBD-14:0,14:0 PE prefers the lo phase, whereas *N*-Rh-14:0, 14:0 PE prefers the ld phase). Donor decays (both in presence and absence of acceptor) were successfully analyzed, from a statistical point of view, using the formalism outlined above. For $x_{chol} = 0.25$, corresponding to high lo phase fraction X_{lo}, acceptor coefficient values calculated from FRET decay parameters using Eq. 13 compared well with those retrieved from variation of fluorescence intensity, indicating validity of the infinite-phase-separation assumption. However, for $x_{chol} = 0.15$ and 0.20, corresponding to lower X_{lo}, the FRET-derived K_{pA} values were closer to unity than the non-FRET size-independent values from fluorescence intensity variation. This behavior was also observed in the analysis of simulated FRET decay data obtained from numerical computation using a distribution of donor and acceptor probes in a lattice made up of small (~3.5–10 R_0) domains. The conclusion was that at variance with the high lo fraction limit, the lo domains distributed in majority ld phase have small size, of the order of a few nm. Support for this also comes from the application of Eqs. 16 and 17 to estimate the phase boundaries from FRET decay data. Whereas the pure lo phase boundary was estimated with excellent agreement with the published phase diagram ($x_{lo} = 0.28$ at $T = 30$ °C for both studies), this was not the case at all for the pure ld phase boundary ($x_{ld} = 0.18$ at $T = 30$ °C from FRET, compared with $x_{ld} = 0.075$ from the aforementioned phase diagram). The significance of this is that FRET is unable to detect phase separation in the $0.075 < x_{chol} < 0.18$ range because lo domains are very small (of the order of R_0 or smaller) for these compositions.

This study served as a blueprint from subsequent estimates of domain size in more complex systems by our group. In these studies, FRET efficiency is typically measured for several points along the phase coexistence tie-line. If the variation in *E* follows that predicted taking into account probe partition and assuming infinite phase separation, then formation of large domains (in the FRET scale) is inferred. Otherwise (e.g., if FRET between probes that have complementary phase preference fails to decrease upon entering the phase coexistence region), formation of small domains is deduced. Using the *N*-NBD-16:0,16:0 PE/*N*-Rh-18:1, 18:1 PE FRET donor/acceptor pair, de Almeida et al. [35] arrived at similar conclusions (small domains in the low X_{lo} range, large domains in the high X_{lo} range) for the 16:0,18:1 PC/*N*-palmitoylsphingomyelin (PSM)/chol raft-mimicking system, allowing rationalization of apparent discrepancies observed in the literature (e.g., 16:0,18:1 PC/chol heterogeneity was detected from size-independent fluorescence spectroscopy data [33, 89], but not from resolution-limited CFM [136]). On the

other hand, Silva et al. [119] detected formation of large ceramide platforms in the 16:0,18:1 PC/palmitoylceramide system using FRET from ceramide gel-located *t*-PnA donor to fluid phase probe *N*-NBD-18:1,18:1 PE.

The approach of measuring the variation of FRET efficiency along a tie-line may also be used to assess the eventual perturbation induced by the addition of a foreign molecule to a given lipid mixture. The effect of physiologically relevant ceramide (Cer) concentrations ($\leq$4 mol %) on the lo/ld coexistence range of the POPC/PSM/chol system was also investigated [120]. For these systems, three donor/acceptor pairs were selected to obtain information regarding (1) ld-lo phase separation, i.e., alteration in lipid raft organization (*N*-NBD-16:0,16:0 PE/*N*-Rh-18:1,18:1 PE); (2) gel-lo phase separation, thus, the organization between the so-called Cer-platforms and lipid rafts (*t*-PnA/ *N*-NBD-16:0,16:0 PE); and (3) gel-fluid (ld + lo) phase separation (*t*-PnA/ *N*-NBD-18:1,18:1 PE). Data obtained for the first pair gave support to the hypothesis of ability of Cer to form gel domains only in the low chol range. Because in the presence of Cer, and in the low chol range, FRET efficiency increased, the inability of Cer to induce the coalescence of raft domains was concluded. Additional topological information of this complex system is obtained with the two other pairs, namely, the size of the gel domains. Because *t*-PnA (donor) has a strong preference toward Cer-enriched gel phases, while both acceptors (*N*-NBD-16:0,16:0 and *N*-NBD-18:1,18:1 PE) are excluded, when gel domains are formed, FRET efficiency decreases. Once again, this was observed for Cer-containing raft mixtures in the low chol range. Because the acceptors are completely excluded from Cer-gel domains, it is possible to estimate the size of the latter assuming that (1) FRET within gel phase does not occur because acceptors are excluded, (2) there is FRET from the gel to the fluid phase, (3) FRET occurs within the fluid phase. Furthermore, it is necessary to take into account the concentration of the donor in each of the phases (determined according to its partition coefficient), the amount of gel phase formed, and the existence of a gel-located donor/fluid-located acceptor exclusion distance, R_e, which was interpreted as an estimate of the gel domain size. It was found that Cer associates with PSM to form small, ~ 4 nm, gel domains. By noting that higher efficiencies were obtained for the *t*-PnA/*N*-NBD-16:0,16:0 pair compared to the *t*-PnA/ *N*-NBD-18:1,18:1 PE pair, and taking into account that *N*-NBD-16:0,16:0 PE prefers lo phase to ld, whereas *N*-NBD-18:1,18:1 PE does not discriminate between these two phases, it was concluded that Cer/PSM-enriched gel domains were surrounded by lo (rather than ld) phase. The foreign molecule may be a peptide or protein, as recently exemplified in a study of the effect of FAS death receptor's transmembrane domain on the domain size of the 16:0,18:1/PSM/chol phase diagram [21].

More recently, other authors have proposed methodologies aimed at the estimation of domain size using FRET. Towles and collaborators published two different analytical approaches recently [15, 132]. These formalisms rely on subtle (but restricting) approximations, which are discussed in detail elsewhere [81].

A convenient way to study the relationship between the FRET observables (donor decay, efficiency) and the domain organization of phase-separated bilayers is the use of numerical simulations. This has been done as a test of the

abovementioned analytical formalisms [74, 79, 131, 132]. In these cases, the simulations were used to test the authors' analytical models and not with the intention of providing fitting equations. This is easily understood noting that there are too many input parameters (domain size and size distribution, domain shape, fraction of each phase, donor and acceptor partition coefficients) to be accommodated by a useful fitting scheme.

Recent simulation works have addressed the limits of FRET in the determination of domain sizes. Using stochastic simulations, Kiskowski and Kenworthy [66] calculated the dependence of FRET efficiency on acceptor concentration for a planar geometry with disklike domains. Two scenarios were considered: co-localization of donors and acceptors inside the domains and segregation of acceptors to the other phase with donors inside the domains. The authors showed that the local acceptor concentration inside the domains (and hence the domain fractional area) could be recovered from the first type of probe distribution, unlike the domain radius. However, the latter could be estimated from the acceptor segregation scenario, namely, for small and intermediate-sized domains. The authors chose to study the extreme situations of co-localization inside the domains (corresponding to domain/continuous phase partition coefficients $K_{pD} = K_{pA} = \infty$) and total acceptor segregation ($K_{pD} = \infty$, $K_{pA} = 0$). However, to model the effect of physical finite K_p values, simulations in which the probes are distributed taking them into account must be performed.

This was fully taken into account in a recent report by Šachl et al. [115]. These authors investigated, using numerical simulations, the feasibility of resolving domain sizes (judged by the resulting ratio between steady-state donor fluorescence intensity in the phase-separated system and that expected for uniform probe distribution) for a variety of K_{pD} and K_{pA} possible values, grouped into three categories: (1) donor/acceptor pairs reside inside lo nanodomains, (2) donor/acceptor pairs are excluded from lo nanodomains, and (3) donors and acceptors exhibit an increased affinity to the different phases. This latter situation (e.g., with lo/ld partition coefficients $K_{pD} = 5$ and $K_{pA} = 0.01$) was revealed as the most favorable, being able to resolve a broad spectrum of nanodomain sizes. However, even in this case, domains that occupy <2.5 % of the overall area and domains with radii $< R_0$ and occupying <10 % of the area were shown to lie beyond experimental resolution (unless K_{pD} increases to values not possible with current probes). On the other hand, currently available donor/acceptor pairs in which both probes prefer the same phase are not feasible for determination of domain sizes < 20 nm.

An altogether different approach was recently applied to the study of the Brain sphingomyelin (BSM) /16:0,18:1 PC/chol study based on a combination of FRET (between 1-[[(6,8-difluoro-7-hydroxy-4-methyl-2-oxo-2 H-1-benzopyran-3-yl)acetyl] oxy]- (Marina Blue-) and NBD-head labeled 16:0,18:1 PE) and statistical mechanical lattice Monte Carlo simulations [45]. For the purpose of FRET efficiency calculation from the simulations, the actual distance dependence of the FRET interaction was replaced by a step function, meaning that FRET was considered to occur if the donor-acceptor distance in a given pair is less than R_0 (4.6 nm). With this simplification and using unlike nearest-neighbor interaction parameters (the only potential

fitting parameters in their Monte Carlo methodology) based on experimental data (and fine-tuned by comparison with the experimental FRET), the authors were able to observe extensive phase separation for BSM/chol/16:0,18:1 PC mole ratio 35:35:30. This agrees with the results of de Almeida et al. [35] described above, which indicate the existence of large ld domains in this lo-rich area of the phase coexistence range. No extensive phase separation is observed in the Monte Carlo simulation of either of the binary mixtures BSM/16:0,18:1 PC 70:30, chol/16:0,18:1 PC 70:30, and BSM/chol 50:50, which, as argued by the authors, agrees with the lack of observation by fluorescence microscopy in GUV of micron-scale phase separation in the binary sphingomyelin/chol, sphingomyelin/16:0,18:1 PC, and chol/16:0,18:1 PC systems, unlike some ternary mixtures of these components.

2.3 Protein-Induced Lipid Distribution Heterogeneity

The studies described in the previous subsections refer mainly to heterogeneity stemming from lipid-lipid interactions. However, proteins are ubiquitous in biological membranes and, as mentioned in Sect. 1, differential protein-lipid interactions may cause nonuniform distribution of lipid components in the bilayer. Several approaches described in the literature that use FRET to characterize this effect were critically reviewed recently [82]. Here we focus on the models proposed by our group and their applications to three different protein systems.

2.3.1 M13 Major Coat Protein

M13 major coat protein (M13 MCP) is the main component of the M13 bacteriophage coat and in its mature form is a polypeptide chain 50 amino acids long, presenting three domains which are expected to be required for the multiple interactions that this protein establishes during the bacteriophage reproductive cycle: (1) a single hydrophobic transmembrane segment of 20 amino acid residues, (2) an amphipathic N-terminal arm, (3) and a heavily basic C-terminus with a high density of lysine residues [49, 127]. ESR and fluorescence studies making use of site-directed labeling of MCP [124, 126] allowed to conclude that Thr36 is located in the center of the bilayer in 1,2-dioleoyl-*sn*-glycerol-3-phosphocholine (DOPC) and 1,2-dioleoyl-*sn*-glycerol-3-[phospho-*rac*-(1-glycerol)] (DOPG) bilayers, while aminoacids 25 and 46 delimit the transmembrane domain boundaries of MCP.

Insertion of M13 MCP in the bilayer milieu is expected to induce a packing stress at the protein-lipid interface and this stress is lessened by some adaptations of the protein [67]. However, the ability of M13 MCP to adapt to situations of hydrophobic mismatch is limited, and in extreme cases aggregation can occur [41]. In the case of complex lipid mixtures, it is energetically favorable to have a distinct lipid composition in the immediate vicinity of the protein that minimizes mismatch stress. Additionally, electrostatic effects can also drive enrichment of particular lipids around the protein. The lipid composition of the inner membrane of

noninfected *Escherichia coli* is about 70 % of phosphatidylethanolamine (PE), 25 % of phosphatidylglycerol (PG), and 5 % cardiolipin (CL). During the infection of *Escherichia coli* by the M13 bacteriophage, the levels of anionic lipids in the cell membrane are slightly increased [109], suggesting that anionic phospholipids assist in the maintenance of a functional state for M13 MCP [49].

From ESR studies, it was known that some regularity exists in the number of immobilized lipids per protein transmembrane segment. The value recovered for this stoichiometry was 12, meaning that only the first layer of lipids around a transmembrane segment is expected to be significantly immobilized by interaction with the protein (assuming a hexagonal arrangement) [88]. Lipids in this layer are entitled annular lipids. Spin-labeled lipids found further away from this shell, although possibly affected by the presence of the protein segment, are not submitted to sufficient dynamic restriction to be detected by the ESR technique. ESR studies with M13 MCP were unable to detect significant immobilization of spin-labeled phospholipids by monomeric M13 MCP [150]. On the other hand, oligomeric MCP immobilized a population of phospholipids, especially at very high protein concentrations [104]. This suggests that a single transmembrane segment inserted in the membrane is unable to sequester a long living lipid shell around it, at least in the ESR timescale.

The hydrophobic surface of a membrane protein is not smooth and the interface between the protein and the lipids surrounding it is likely to be heterogeneous [71]. On the other hand, the largely fixed stoichiometry for annular lipids denotes some ordering in the protein-lipid interface. In this way, it is possible to describe this annular shell in terms of a uniform surface for which 12 identical binding sites are available [88], and the process has been described as competitive binding of lipids to the protein surface binding sites [71, 98, 111, 144].

FRET experiments assuming this model were applied to the study of the affinity of M13 MCP to different lipid classes and chain lengths [42]. The M13 MCP behavior in the membrane is extremely well resolved, especially in regard to its positioning in the lipid environment, and for that reason M13 MCP was a particularly attractive subject for the application of FRET as recovering quantitative information for protein-lipid selectivity requires some degree of parameterization. For the experiments, a M13 MCP mutant for which the Thr36 (located in the center of the bilayer) was changed to a cysteine was specifically labeled at this position with a coumarin fluorophore. Protein was then incorporated in liposomes composed of unsaturated phosphocholines of different thickness, loaded with different concentrations of *N*-NBD-18:1,18:1 PE, which acts as a FRET acceptor for coumarin, the FRET donor. FRET efficiencies were calculated from the integration of the donor fluorescence decays and the data were analyzed on the basis of a model which assumed two populations of energy transfer acceptors, one located in the annular shell around the protein, whose composition is determined by protein-lipid interactions, and the other outside it, with a random distribution unaffected by the protein. Due to the large R_0 of the coumarin and NBD pair (~39.3 Å), the donor fluorescence decay curve had energy transfer contributions from both of these acceptor populations:

$$i_{DA}(t) = i_D(t)\rho_{\text{annular}}(t)\rho_{\text{random}}(t) \tag{18}$$

here, ρ_{annular} and ρ_{random} are the FRET contributions arising from energy transfer to annular labeled lipids and to randomly distributed labeled lipids outside the annular shell, respectively. All annular acceptors were assumed to be at the same distance (d) to the coumarin fluorophore in the center of the transmembrane domain, and FRET to each of these acceptors was associated with the rate constant given by Eq. 1, with $R = d$. The probability of each of the 12 annular sites to be occupied by an acceptor depends on the acceptor molar fraction and on a relative selectivity constant (K_S) which quantifies the relative affinity of the labeled to unlabeled phospholipids:

$$\mu = K_S \frac{N_{\text{Acceptor}}}{N_{\text{Acceptor}} + N_{\text{Unlabeled lipid}}} \tag{19}$$

where N_{Acceptor} is the concentration of labeled lipid and $N_{\text{Unlabeled Lipid}}$ is the concentration of unlabeled lipid. A binomial distribution describing the probability of each occupation number assuming a given μ (0–12 sites occupied simultaneously by labeled lipid) is considered for the calculation of ρ_{annular}:

$$\rho_{\text{annular}} = \sum_{n=0}^{12} e^{-nk_T t} \binom{12}{n} \mu^n (1-\mu)^{12-n} \tag{20}$$

On the other hand, the FRET contribution arising from energy transfer to non-annular lipids, ρ_{random}, was dictated by Eq. 8, where R_e was calculated from the expected exclusion distance between the protein and lipids outside the annular shell (sum of protein and 1.5 lipid radii to account for exclusion effect of annular lipids) and the separation between donor and acceptor planes in the bilayer. NBD fluorophore position in the membrane is known to be close to the surface for phospholipid labeling in both headgroup and acyl-chains and has been determined through several techniques [1, 23, 75, 91].

The value for NBD-labeled lipid concentration outside the annular region (c) was also corrected for the presence of acceptors inside the annular region. Eqs. 1, 8, 18, 19, and 20 were then used to simulate donor decay curves under FRET, and FRET efficiencies were calculated from numerical integration of these curves (Eq. 9). During fitting of this model to experimental data, the only variable was K_S. This model was applied to the analysis of protein preference for acyl chain thickness and headgroup selectivity. In the first set of experiments, the same headgroup-labeled lipid *N*-NBD-18:1,18:1 PE, with perfect hydrophobic matching to the M13 MCP, was added to proteoliposomes presenting different lipid membrane thickness and coumarin-MCP. Coumarin-MCP quenching due to FRET to NBD-labeled lipids was measured and the selectivity model was fitted to the data. Different K_S values were recovered for *N*-NBD-18:1,18:1 PE depending on the thickness of the bulk lipid used. M13 MCP presented higher affinity for *N*-NBD-18:1,18:1 PE when there was considerable mismatch between the protein and the

bulk lipid, reflecting an enrichment of the hydrophobically equivalent lipid in the annular shell of the protein, minimizing in this manner the hydrophobic mismatch stress in the protein-lipid interface.

The same method was used to determine the selectivity of the protein for different phospholipid headgroups in a second set of experiments. This time, different acceptors were used and all studies were carried out in 18:1,18:1 PC. The probes used as acceptors were phospholipids of identical acyl-chains (18:1 and 12:0) belonging to different phospholipids classes (PE, PC, phosphatidylglycerol (PG), phosphatidylserine (PS), and phosphatidic acid (PA)) labeled with NBD at the shorter acyl-chain (18:1,NBD-12:0 PE, PC, PG, PS, and PA). Larger K_S values were recovered for anionic labeled phospholipids, particularly for PA ($K_S = 3.0$) and PS probes ($K_S = 2.7$). The PG lipid presented an intermediate affinity for the annular shell of lipids ($K_S = 2.3$) whereas PC and PE probes induced less energy transfer reflecting lower K_S values ($K_S = 2.0$ for both). Selectivity for anionic phospholipids is a consequence of electrostatic interaction of these with the lysine-rich C-terminal domain of the protein. Even though the protein is shown to present higher affinity for the labeled lipid than for the bulk lipid ($K_S > 1$), possibly as a result of electrostatic interactions with the NBD group, this method was further validated by the fact that the relative association constants [$K_S/K_{S(\text{PC labeled lipid})}$] obtained were almost identical to the values obtained with ESR and the aggregated form of the protein [104].

In this experiment, as a result of the low selectivity character of the M13 MCP protein–annular lipid interaction and the large coumarin-NBD R_0, FRET contribution from noninteracting acceptors clearly dominates over annular acceptor contribution. This significantly reduced the sensitivity of the method, and nearly error-free measurements of FRET efficiency and acceptor concentration are required for the recovery of accurate selectivity constants. This limitation can be bypassed through the use of donor-acceptor pairs presenting lower R_0 for which FRET due to acceptors in the annular shell will become more predominant.

2.3.2 Lactose Permease

Lactose permease (LacY) of *Escherichia coli*, one of the most intensively studied membrane proteins, is often taken as a paradigm for secondary transport [54]. It consists of 12 transmembrane α-helices, crossing the membrane in a zigzag fashion. LacY translocates the substrate (specifically disaccharides containing a D-β-galactopyranosyl ring) with H^+, in a symport (cotransport) reaction. It was pointed out early [24] that the amino groups of phospholipids such as PE are of crucial importance for LacY function. More recently, it has been conclusively demonstrated that LacY requires the presence of PE for its correct folding in the membrane during biogenesis [9], its function in vivo, [8] and to maintain its correct topology [10, 11]. In particular, LacY is fully functional when reconstituted in mixtures of 16:0,18:1 PE/16:0,18;1 PG. FRET experiments were used to elucidate whether one of these phospholipids is enriched in the annular region of LacY [108]. W151 of LacY was used as donor and two different pyrene-labeled phospholipids

(a PG analog, 16:0, pyrene-10:0 PG (Pyr-PG), and a PE analog, 16:0, pyrene-10:0 PE (Pyr-PE)), were chosen as acceptors. Additionally, the effect of cardiolipin (CL) on the annular lipid composition was also investigated.

FRET efficiencies were analyzed essentially as described for M13 MCP, with the difference that, due to the size of the protein, the number N of annular sites available is now much larger (46 (23 in each leaflet) instead of 12; [108]). The donor LacY W151 was assumed to be located in the axis of the cylindrically symmetrical protein, near the membrane interface. All acceptor fluorophores were assumed to be located near the center of the bilayer. In this way, the distance between donor and annular acceptor molecules was taken as identical for all annular acceptors, independently of their membrane leaflet. Using l =1.2 nm as the transverse distance between W151 and the acceptor plane and R_e = 3.0 nm as the exclusion distance along the bilayer plane between the protein axis and the annular lipid molecules, the donor–annular acceptor distance is given by $R = (l^2 + R_e^2)^{1/2}$ = 3.2 nm. For the Förster radius, the value R_0 = 3 nm, reported for the Trp/pyrene pair [130], was used, whereas for the calculation of n_2, area/lipid values of 0.56, 0.56, and 1.26 nm^2 were assumed for 16:0,18;1 PE; 16:0,18;1 PG; and CL, respectively [55, 112].

Experimental FRET efficiencies between the single Trp151 of LacY and either Pyr-PG or Pyr-PE as acceptors were measured in the different lipid systems (16:0,18:1 PE/16:0,18:1 PG; 18:1,18:1 PE/16:0,18:1 PG; and 16:0,16:0 PE/16:0,18:1 PG, all 3:1) at 37 °C, in order to recover the best fit values of the model parameter μ. This parameter represents the probability of finding a given phospholipid in the annular region of LacY. The fact that higher FRET efficiencies are obtained for transfer to Pyr-PE (0.232 ± 0.028) compared to Pyr-PG (0.165 ± 0.018) in the 16:0,18:1 PE/16:0,18:1 PG system, and, in a similar way for Pyr-PE (0.231 ± 0.023) compared to Pyr-PG (0.211 ± 0.038) in the 18:1,18:1 PE/16:0,18:1 PG system, is a first indicator of the selectivity of LacY for PE relative to PG in these systems. This is confirmed by the quantitative model calculations. Best agreement with experimental values requires an annular region composed of approximately ~90 mol% PE in these systems, whereas 75 mol% would be expected for random distribution of both phospholipids. In the 16:0,18:1 PE/16:0,18:1 PG mixture, the FRET data are compatible with complete PG exclusion from the annular layer, which is therefore composed solely of PE (μ(PE) = 1.00, μ(PG) = 0.00). Notably, when LacY is reconstituted in 18:1,18:1 PE/16:0,18:1 PG, the experimental FRET efficiencies indicate an enrichment of PG in the annular region (μ(PE) = 0.86, μ(PG) = 0.14), but still in lower concentration than expected for uniform lipid distribution. Regarding the 16:0,16:0 PE/16:0,18:1 PG mixture, gel/fluid phase coexistence is expected, with 16:0,18:1 PG-enriched fluid domains coexisting with 16:0,16:0 PE-enriched gel-phase bilayer regions. In this system, an increase in the efficiency of FRET to Pyr-PG and a decrease in that to Pyr-PE are verified, to an extent that the efficiency of FRET to Pyr-PG now clearly surpasses that to Pyr-PE. This is a clear indication that LacY is preferably located in the fluid domains, where the PG acceptor probe is more abundant.

In addition to PE and PG, the lipid composition of *E. coli*'s membrane contains 5 % to 7 % of CL. To test the effects of this phospholipid on the annular region, 14:0 CL and 18:1 CL were incorporated in the 16:0,18:1 PE/16:0,18:1 PG matrix. Incorporation of CL decreases the efficiencies of FRET when comparing to the same phospholipid mixtures containing no CL, especially when the acceptor is Pyr-PG. This suggests that CL displaces 16:0,18:1 PE and, more extensively, 16:0,18:1 PG from the annular region of LacY. The fact that the effect is more pronounced for PG than for PE is probably related to the preference of the protein for PE species as described above for the binary systems. Upon applying the FRET quantitative model, when the acceptor is Pyr-PG, even by imposing segregation of this probe from the first annular layer ($\mu(PG) = 0$), it is still not possible to conciliate the theoretical (0.162) and the experimental values (0.143 for 18:1 CL, 0.142 for 14:0 CL). This indicates that besides being totally excluded from the first layer, PG is also somewhat rarefied beyond it. On the other hand, when the acceptor is Pyr-PE, a model matching to the experimental efficiencies (0.183 for 18:1 CL, 0.196 for 14:0 CL) requires only partial replacement of PE by CL. When the CL lipid is 18:1 CL, the retrieved composition of the annular layer is 40 mol% PE and 60 mol% CL. On the other hand, when the CL lipid is 14:0 CL, the composition of the annular layer is 68 mol% PE and 32 mol% CL, indicating that in this case PE is kept in close proximity of the protein, in the same proportion as in the bulk. In the latter case, CL enrichment in the annular layer is solely produced by replacing PG. The fact that 14:0 CL is not able to displace PE in the same way that 18:1 CL does is probably due to the hydrophobic mismatch between the short 14:0 acyl chains and the protein. On the whole, this study confirms that PE is the most relevant component of the annular region and that, because it is not displaced by PG or (completely) by CL, it appears to be tightly bounded to LacY. Selectivity of LacY for PE and predominance of this phospholipid at the annular region, verified and characterized by FRET measurements and modeling, provide support for a hypothetical coupling between this lipid and LacY during the transport cycle.

The work described above was carried out mostly in PE/PG 3:1 mixtures, a ratio identical to that found in the inner membrane of *E. coli* [40]. This creates a dilution problem. For example, in an experiment where the acceptor is labeled PE, even if the annular region would be solely comprised of PE lipid, the enrichment of labeled PE in this layer would be only of a factor 4/3. Adding to the fact that unspecific FRET to acceptors outside the annular layer is always present, this would imply a rather modest increase in the expected FRET efficiency. Finally, the simple fact that a pyrene acyl chain–labeled lipid behaves identically to unlabeled lipid of the same class is questionable, and this cannot be resolved in an experiment where the host lipid matrix is a two-component mixture. For these reasons (to gain increased sensitivity and to assess the extent of correct reporting by the acceptor probes of each class), this protein system was readdressed in a recent work [129], using different one-component host lipid matrices. Besides, the influence of headgroup and acyl chain composition was also investigated.

In Table 1, the experimental FRET values are listed along with the calculated μ and K_s values. As can be seen, the probability of finding labeled phospholipids at

Table 1 Probabilities of each site in the annular ring being occupied by a pyrene-labeled phopholipid and relative association constant toward LacY, as determined by FRET. Reprinted from Suárez-Germà et al. [129] with permission. Copyright 2012 American Chemical Society

		16:0,18:1 PE matrix			16:0,18:1 PG matrix		
	Acceptor	μ	K_s	K_s/K_s(PE)	μ	K_s	K_s/K_s(PE)
25 °C	Pyr-PE	0.10	6.53	1.00	0.03	2.00	1.00
	Pyr-PG	0.00	0.00	0.00	0.00	0.00	0.00
	Pyr-PC	0.00	0.00	0.00	0.00	0.00	0.00
37 °C	Pyr-PE	0.08	5.53	1.00	0.04	2.47	1.00
	Pyr-PG	0.00	0.00	0.15	0.00	0.00	0.00
	Pyr-PC	0.02	1.40	0.25	0.03	2.00	0.81

the annular regions (μ) is always the highest, irrespectively of the matrix, for Pyr-PE. This behavior reflects the values of the FRET efficiency mentioned above. By inspecting the outcome for K_s values, we notice that the largest values are obtained for Pyr-PE in all matrices and both temperatures. It is worth mentioning that ideally $K_s = 1$ for any probe that mimics the non-labeled phospholipids and values between 1 and 3 have been reported (as measured for FRET between labeled M13 MCP and NBD lipids as described above; [42]). Therefore, these high values of K_s obtained for Pyr-PE may indicate either an annular region extremely enriched in the label or that Pyr-PE does not mimic well the unlabeled phospholipid. Although this may be a handicap, if one compares across probes in the same host lipid, it becomes clear that there is an effect of preference of Lac Y for PE over PG and PC. Since the probes are all equal except for the headgroup, and for comparing the different probes in the same host lipid, K_s/K_s(PE) ratios are provided in Table 1.

In the 16:0,18:1 PE matrix, μ values indicate that Pyr-PG is excluded at both temperatures and that 16:0, pyrene-10:0 PC (Pyr-PC) is excluded at 25 °C and shows a small enrichment at 37 °C. Since $K_s = 0$ means no acceptor in the annular region, it becomes clear that at 25 °C, Pyr-PG and Pyr-PC are completely excluded. While Pyr-PG behaves in the same way at 37 °C, LacY shows an increased preference for Pyr-PC at this temperature. The overall results in the 16:0,18:1 PE matrix, where LacY is folded closely to the in vivo conditions, point to the fact that Pyr-PE should be in closer proximity than the other labels. On the other hand, μ and K_s for Pyr-PE in the POPG matrix are compatible with a moderate enrichment of the label in the annular region. Pyr-PG is depleted from the annular region at both temperatures when the host phospholipid is 16:0,18:1 PG. Similarly, we can observe that Pyr-PC is also depleted when hosted by 16:0,18:1 PG at 25 °C and that a very slight enrichment is observed at 37 °C. All these observations may be likely related with the inverted topology of domains C6 and P7 of LacY when reconstituted in POPG proteoliposomes [12]. Our FRET measurements in 16:0,18:1 PE and 16:0,18:1 PG matrices confirm the preference of LacY for PE and its probable predominance in the annular ring [108]. This may support, indirectly, a hypothetical interaction between the PE headgroup and some specific residue of the protein [24, 123]. Importantly, recent observations have shown that uphill transport

occurs in *E. coli* in which PE has been completely exchanged by PC [13]. Since in PE and PC matrices LacY exhibits its natural topology, this intriguing observation pointed out to a more complex molecular interaction between the protein and the annular phospholipids. Hence FRET measurements in PC matrices become of interest given the fact that despite its natural topology in these matrices, LacY only shows downhill transport in 18:1,18:1 PC proteoliposomes [142]. Pyr-PG is slightly enriched in the annular region when the matrix is 18:1,18:1 PC ($K_s > 1$) but excluded from it in a 16:0,18:1 PC matrix ($K_s \sim 0$). However, the most interesting result is possibly that, according to the K_s values, Pyr-PC is enriched in the annular region in a 16:0,18:1 PC matrix ($K_s > 1$) and excluded from it in a 18:1,18:1 PC matrix ($K_s \sim 0$).

Given that 18:1,18:1 PC and 16:0,18:1 PC share the same headgroup and have very similar hydrophobic lengths in the bilayer (2.48 vs. 2.54 nm, respectively; [123]), this difference is probably related to the different specific curvature of the two lipid species. It has been reported that whereas proper topology of LacY depends on a dilution of high negative surface charge density (and hence probably the decreased affinity of the protein for PG), rather than on spontaneous curvature (C_0; [11]), the latter appears to be crucial regarding uphill transport of lactose by LacY in vivo [143], with negative curvature lipids like PE being required. C_0 (16:0,18:1) is essentially zero, while 18:1,18:1 PC, due to its additional unsaturated acyl chain, has a negative specific curvature (C_0(18:1,18:1 PC) $= -0.11$ nm^{-1}; [123]). Although its value is still far from the non-bilayer lipid 18:1,18:1 PE (C_0(18:1,18:1 PE) $= -0.35$ nm^{-1}; [123]), it may justify the preference of properly reconstituted LacY for 18:1,18:1 PC rather than 16:0,18:1 PC, and hence the differential behavior in these two PC matrices regarding selectivity for labeled probes.

2.3.3 Pulmonary Surfactant Protein SP-B

Pulmonary surfactant is composed of roughly 90 % lipids and 8–10 % of specific surfactant-associated proteins, termed in chronological order of discovery SP-A, SP-B, SP-C, and SP-D [61]. The most abundant phospholipid species in surfactant is 16:0,16:0 PC, which is also the main surface-active component [26, 97]. However, it is clear that surfactant lipids are not able by themselves to reach rapidly the air/liquid interface as they are secreted by type II pneumocytes, to form operative surface-active films. Presence of hydrophobic surfactant proteins SP-B and SP-C is strictly required to facilitate an efficient transfer of phospholipids from surfactant stores (in the form of bilayers) at the aqueous hypophase into the interfacial film, along the breathing cycles [105, 106]. However, the molecular mechanisms by which surfactant proteins participate in the assembly, transport, and reorganization of surfactant lipids at the respiratory surface are still not well understood.

Mature SP-B is a 79-residue polypeptide, which comes from the proteolytic maturation of a longer precursor of 381 amino acids (42 kDa) produced in type II cells. SP-B processing is coupled with the assembly of surfactant membranes into lamellar bodies, the specific surfactant-storing organelles in pneumocytes. In the

native form, SP-B contains intramolecular and intermolecular disulphide bonds stabilizing a homodimeric structure [62]. The three-dimensional structure of SP-B has not been yet determined.

The essential role of SP-B in surfactant has been related with the ability of the protein to promote a rapid transfer of phospholipids into air-water interfaces. SP-B, therefore, could be required to establish an operative surface active film from the earliest air-liquid respiratory interface. SP-B has been described to promote more or less deep perturbations in membranes leading to lipid exchange and eventual fusion between liposome membranes and rapid leakage of their content [100, 110, 114]. The elucidation of the mode and extent of interaction of SP-B with surfactant membranes and films is therefore important to fully understand its structure-function relationships. The in-depth location and orientation of SP-B in phospholipid membranes as reconstituted in vitro has been a matter of controversy. On the one hand, evidence suggests that SP-B is located in a shallow region of membranes, with the polar positively charged sides of the helical segments interacting with anionic phosphatidylglycerol (PG). This superficial lipid-protein interaction would produce little perturbations on the acyl chain packing of surfactant phospholipids [94, 99, 133]. Other experiments, in contrast, have reported significant effects of SP-B on acyl chain order, consistent with a deeper penetration of SP-B in membranes and a direct perturbation by the protein of their hydrophobic core [39, 107, 118]. On the other hand, the extent of perturbation by SP-B of the structure and thermotropic properties of phospholipid membranes resulted to be critically dependent on the method used to reconstitute the lipid/protein complexes [28]. A matter of discussion has also been the occurrence of selective interactions between SP-B and anionic phospholipids in surfactant, such as phosphatidylglycerol (PG). Inclusion of different phospholipid spin probes in membranes allowed to determine that SP-B shows a preferential interaction with PG in membranes, compared with other zwitterionic or anionic species, as analyzed by electron spin resonance (ESR) spectroscopy [29, 107]. Other studies, however, have suggested that SP-B may prefer to partition into DPPC-enriched rather than DPPG-enriched regions in interfacial films, as detected by TOF-SIMS analysis of lipid/protein films transferred onto solid supports [14, 116].

Fluorescence from the single tryptophan (W9) in the sequence of SP-B was used to get further insight on the location, orientation, and structural dynamics of SP-B in different membrane environments, as well as on the existence of possible selective interactions between SP-B and particular phospholipid species, using FRET to NBD-labeled phospholipid probes [20]. Two different theoretical models could describe the two main possible protein arrangements in the membrane.

In model I (Fig. 5a), a deep embedment of the protein in the membrane would create an area of exclusion of phospholipid molecules equivalent to the surface taken by the protein. A topologically equivalent situation would be that originated if the protein dimer could span the whole bilayer thickness, as proposed in certain models [147]. Donor quenching by FRET in this first model could arise from two distinct acceptor populations: one located in a single circular layer of annular lipid surrounding the protein, and another uniformly distributed beyond the annular region.

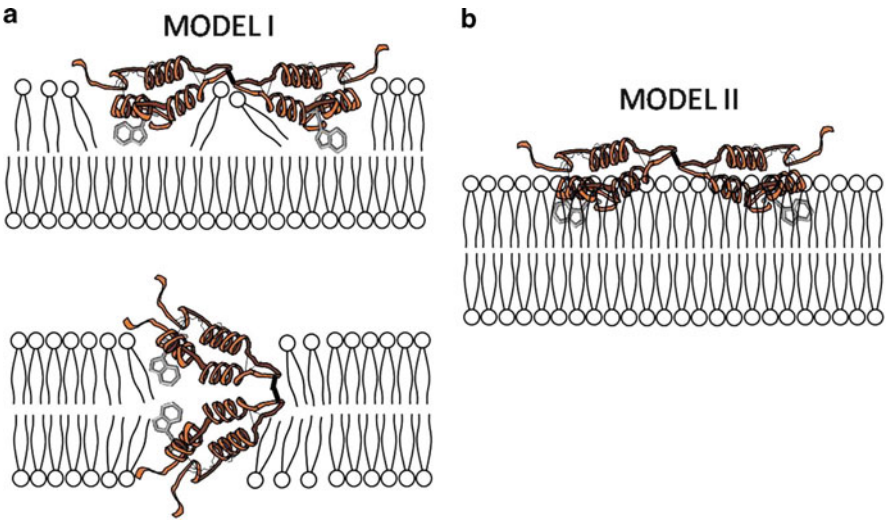

Fig. 5 Theoretical molecular models for the topology of SP-B in phospholipid membranes. *Panel a* represents model I, where the protein insertion leads to an area volume exclusion in the membrane occupied by the protein instead of lipids (and therefore represents an exclusion area for FRET acceptors). *Panel b* represents model II, where the protein exhibits a shallow interaction with the membrane surface, with no lateral lipid excluded area. Single FRET Donors (Trp residues) per SP-B monomer are indicated (Reprinted from Cabré et al. [20] with permission. Copyright 2012 Elsevier)

The formalism for this molecular arrangement is readily adaptable from the one used in the previous examples. However, it was verified that the theoretical efficiency obtained with this formalism is very low when compared with the experimental measurements for reasonable values of the model parameters. For this reason, this model was discarded in the quantitative analysis of lipid selectivity.

Model II (Fig. 5b) assumes that the protein adsorbs to the membrane surface. FRET can again occur to two distinct acceptor populations, one located directly below the protein (where the possibility of acceptor enrichment due to protein-lipid selectivity is considered) and another, located beyond this region (bulk bilayer). Derivation details of this model are presented elsewhere [20]. Despite the difference in topology, the main fitting parameter in this formalism is again a selectivity constant K_s, which is a measure of the preference of the protein for a given acceptor to be located underneath, over the host lipid.

The experimental FRET efficiencies were obtained in these experiments from the measured quenching of donor fluorescence, in 50 mM Hepes buffer, pH 7.0, in the absence of salt or in the presence of 150 mM NaCl. Fig. 6a illustrates how at low salt content, FRET from SP-B tryptophan is less efficient toward zwitterionic NBD-PC than to the negatively charged species NBD-PG or NBD-PS. Similar

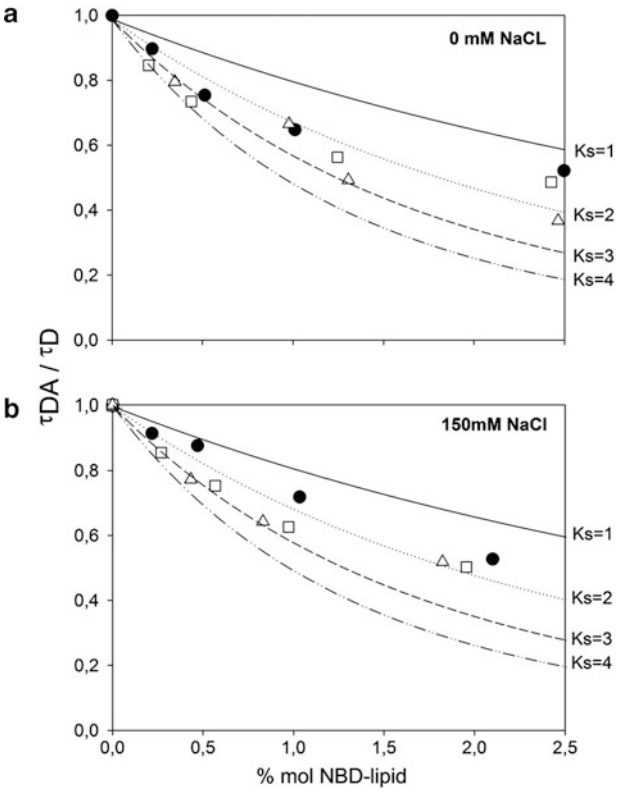

Fig. 6 Donor (SP-B tryptophan) fluorescence quenching by FRET acceptor (NBD-lipids) in a 16:0,18:1 PC membrane matrix. Experimental time-resolved FRET data have been obtained in 50 mM Hepes buffer, pH 7.0, at low (0 mM NaCl, *panel a*) or physiological (150 mM NaCl, *panel b*) ionic strength. Acceptors were NBD-PC (*closed circles*), NBD-PG (*squares*), or NBD-PS (*triangles*). Lines are the theoretical curves for the different indicated selectivity constant K_s values, which consider the topology of the protein in the membrane (model II; see Fig. 3) (Reprinted from Cabré et al. [20] with permission. Copyright 2012 Elsevier)

trends are observed at physiological ionic strength (Fig. 6b). In contrast to the data previously reported using spin-labeled lipids [107], significant differences in selectivity between PG and PS could not be detected. The experimental data obtained for FRET from SP-B to NBD-labeled lipids have been compared in Fig. 6 with the theoretical behavior expected considering a random distribution of donor and acceptor probes in the membranes. As shown in Figs. 6a and b, the selectivity parameter $K_s = 1$ plots still predict less FRET efficiency than measured experimentally, even for the zwitterionic probe NBD-PC, and some degree of probe preference must be invoked (the experimental data are in fact closer to the $K_s = 2$ curves), similarly to the previous examples.

3 Microscopy Studies Using FRET to Probe Lateral Heterogeneity

Recent developments in multiwavelength and polarization-resolved imaging have led to a widespread use of FRET imaging in studies of functional assemblies in cell membranes. The experimental methods for visualizing membrane microdomains and quantifying FRET efficiencies in FRET microscopy with emphasis on novel strategies have been reviewed elsewhere [60, 101, 103, 113]. Several approaches were developed in order to explore, on the nanoscale range, specific protein-protein, lipid-lipid, or lipid-protein interactions in live cells, both using homo- and hetero-FRET.

Cell membranes are characterized by a large number of lipid and protein components in a nonequilibrium state. One common simplification is to assume two types of domains, e.g., raft/non-raft or ordered/disordered. The results can then be compared to, e.g., the ld/lo coexistence on a lipid phase diagram in a ternary model system. Due to intrinsic limitations such as cell stability, and because usually in cells microscopy studies are carried out (in order to control cell state, to know the fluorophore localization, and use the signal coming only from the membrane of interest) fluorescence intensity decays with a high number of photons and low background signal (necessary to the applications of most of the formalisms described above) are generally unfeasible. Usually, steady-state data is obtained and compared to an integrated FRET formalism. Even when Fluorescence Lifetime Imaging Microscopy (FLIM; see Stöckl and Herrmann [125] for a review of its applications to membrane heterogeneity) lifetime data is obtained (FRET-FLIM), a relatively low number of counts is often obtained, which implies that the decay is traditionally used to calculate FRET efficiency using Eq. 9, rather than being directly analyzed with the underlying FRET kinetic model. However, with instrumental improvements as well as development of novel analysis approaches [53], this trend is being reversed. Selected works combining FRET and microscopy are listed in Table 2, which succinctly describes illustrative literature reports in which FRET was used in characterization of membrane domains, protein/lipid selectivity, or protein oligomerization.

In addition to the usual advantages of time-resolved methodologies such as independence on local probe (donor) concentration, under the microscope FRET-FLIM is a method of choice, since it is much less affected by artifacts, and direct information on the FRET efficiency is obtained, without the more complex approaches used in steady state, such as the so-called filter cube FRET microscopy. Additionally, this one also relies on FLIM for the determination of correction factors related to intensity determinations. One example of a relevant FRET-FLIM application, even in the framework of a low time-resolution approach (time-gated detection),

Table 2 Selected examples of FRET microscopy membrane studies

[65]	Clustering of the GPI-anchored protein 5′ nucleotidase was not detected using FRET between labeled antibodies
[135]	Clustering in domains with less than 70 nm of a glycosylphosphatidylinositol (GPI) anchored protein at the cell surface detected by homo-FRET
[56]	FRET-FLIM study of the raft-dependent interaction of tetanus neurotoxin with Thy-1
[57]	Suggestion of preferential interaction of phospholipase D with PC, rather than PE – a qualitative FLIM study
[117]	Characterization of size of lipid-dependent organization of GPI-anchored proteins in live cells, using homo- and hetero-FRET
[141]	FRET-FLIM revealed interaction between BACE (β site of amyloid precursor protein-cleaving enzyme) and the LDL receptor–related protein occurring on lipid rafts at the cell surface
[2]	Improved model for analysis of FRET adapted to the case where D and A label two probing proteins. Application to the data of [65] gave quantitative support to the presence of lipid rafts
[93]	Quantitative study of the distribution of functional neurokinin-1 receptors in the plasma membrane. The receptors are found to be monomeric and reside in membrane microdomains of size below optical resolution
[5]	Derivation of a model considering intramolecular and/or intermolecular FRET and oligomerization, and its experimental verification. Discussion of the effect of cell fixation.
[47]	Cortical actin activity regulates spatial organization of nanoclusters of GPI-anchored proteins at the cell surface, as shown by homo-FRET
[50]	FRET-FLIM revealed that ganglioside GM1 co-localizes with EGF receptor, but not with the non-raft transferrin receptor

is the study related to the localization of the epidermal growth factor receptor (EGFR) in membrane rafts [50]. These authors observed a decrease on fluorescence lifetime of the receptor derivatized with fluorescent antibodies (Alexa 488), in the presence of the typical raft marker GM1(labeled with cholera toxin-A594; Fig. 7). The study was carried out with the two fluorescent antibodies (Fig. 7a, b) in order to discard any specific effect that could be invoked regarding the first antibody, and similar FRET efficiencies were observed in both cases. The result depicted in Fig. 7c is the negative control of the previous experiments. In this case, the labeled donor is the transferrin receptor (Tf-A488), which is known not to partition into rafts, and this rules out the hypothesis that in the previous experiments, the known artifact of GM1 clustering was biasing the data. Interestingly, no significant interaction of EGFR with another well-known raft marker, GPI (glycosylphosphatidylinositol), in this case with GFP (green fluorescent protein), was observed (Fig. 7d). It should be stressed that FRET is essential to clearly demonstrate interaction at the molecular scale, since pixel co-localization cannot be used due to the restricted low lateral resolution of conventional microscopy, as compared to the molecular range of distances.

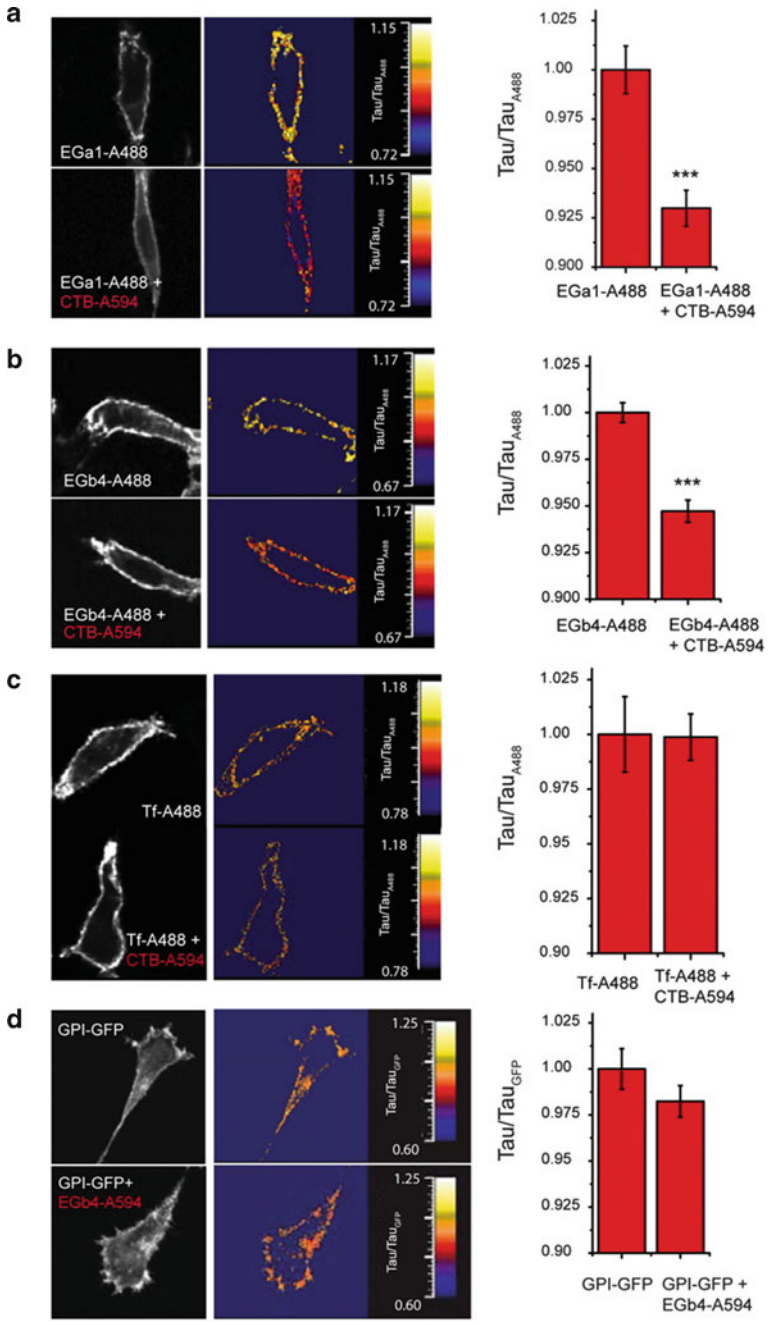

Fig. 7 Nanoscale co-localization of EGFR with GM1 gangliosides from FRET-FLIM data. (**a**–**c**) HER14 cells grown on coverslips were incubated on ice with 100 nM (**a**) of the donor probes anti-EGFR nanobody EGa1 or (**b**) EGb4 directly conjugated to Alexa-Fluor-488 or with (**c**) 20 μg/ml

4 Concluding Remarks

In this chapter, applications of FRET in membrane biophysics are described, comprising studies of lateral heterogeneity (membrane domains) and determination of protein/lipid selectivity (preference of a specific lipid for the protein vicinity). The complexity of FRET in membranes was addressed, and detailed topological information can be obtained from this methodology, once adequate modeling is taken into account. Examples of relevant works in this area are described. On the whole, the power of FRET as a tool in the characterization of membrane component lateral distribution is emphasized.

FRET combines the unique sensitivity of fluorescence with a steep dependence on distance and local concentration, which in turn is reflected on an ability to detect heterogeneity on a length-scale unavailable to other techniques. However, to make the most of FRET's potential, some points should be taken into account. Simulation studies described in this chapter have revealed that for optimal characterization of domain structure, probe partition between the coexisting domains should be complementary. In this way, when designing a FRET experiment for investigation of domain structure, it is important to consider/anticipate the nature of the coexisting phases and select them accordingly. Most probes prefer fluid, disordered phases (e.g., Rh-PE, NBD-PC, *N*-NBD-PE with short or unsaturated acyl chains). A good gel-phase probe is *t*-PnA, whereas head-labeled NBD-PE probes with long saturated acyl chains are convenient lo reporters. Therefore, *t*-PnA/NBD-PC (gel/ld), *t*-PnA/*N*-NBD-PE (gel/ld, gel/lo), and *N*-NBD-PE/Rh-PE (lo/ld) constitute useful FRET pairs.

Regarding domain detection/characterization, different applications can be envisaged, ranging from the identification of the onset of phase separation/construction of previously unknown phase diagrams to the estimation of domain organization in systems where the underlying phase diagram is known. Naturally, pertinent to this is the question addressed in Section 1 of what constitutes a phase. As illustrated in Sect. 2.2, regarding both binary and ternary mixtures exhibiting ld/lo phase coexistence, FRET cannot detect extremely small domains which may be sensed by distance-independent spectroscopic techniques (such as variation of fluorescence lifetime, quantum yield or anisotropy along a tie-line). However, even in this case, FRET is useful, as it allows concluding that the domains perceived by other techniques have necessarily very small size ($\sim R_0$ or smaller). On the other

Fig. 7 (continued) transferrin-A488 (Tf-A488) in the absence or presence of 1 μg/ml of the acceptor probe CTB-A594. (**d**) HER14 cells expressing GPI-GFP were incubated (GPI-GFP + EGb4-A594) or not (GPI-GFP) for 1 h on ice with 100 nM EGb4-A594 (acceptor). After fixation with 4 % formaldehyde, average fluorescence lifetime values of GFP were determined. *Left panels* represent the distributions of the donor probes with or without acceptor probe. The lifetimes are shown in the *middle panels* in false colors. The histograms on the right are mean fluorescence lifetimes of the probes. See text for details (Reprinted from Hofman et al. [50] with permission. Copyright 2008 The Company of Biologists Limited)

hand, whereas the formalisms presented allow, in favorable cases, estimation of average domain size, polydispersivity and shape cannot be normally resolved.

Generally, measurement of donor decay in absence and presence of acceptor is preferred to measurement of FRET efficiency from steady-state. Despite being a rapid way of obtaining a first glimpse into the possible membrane organization, the steady-state FRET detection is always limited. The FRET efficiency parameter results from time integration of the actual decay law, and in this process considerable detail regarding the probes distribution is lost. Thus, whenever possible, a complete parameter analysis of the time-resolved fluorescence donor decays should be carried out (ideally with global analysis of samples with and without acceptor. Moreover, time-resolved measurements are less prone to artifacts such as inner filter effects or variations in donor concentration across samples.

The dependence of FRET upon donor-acceptor distance is reflected in a sensitivity to geometry and topology of probe distribution, and, by extension, of the underlying system. Modeling of FRET in most problems in membrane biophysics therefore requires knowledge of structural parameters such as area/lipid, transverse location of fluorophores, or protein dimensions. In favorable cases (i.e., situations in which uniform distribution of donor and acceptor can be safely assumed), the FRET experiment can itself be used to determine some of these parameters. However, in the context of this chapter, which concerns deviations to uniform distribution of membrane components, it is especially important that as much FRET-independent information is used (otherwise precise recovery of the heterogeneity features is impossible). Of course, for many membrane systems this is unfeasible, because of lacking lipid and/or protein structural information. In these situations, estimates are used, which may limit the usefulness of the FRET experiment.

In addition to structure, the dynamic properties of the system under study may also influence the FRET process. In most cases, translational diffusion during the donor excited state is negligible. However, relative fluorophore orientation and rotational diffusion, as expressed in the κ^2 parameter, affects R_0 (Eq. 2) and hence FRET kinetics. Because there is no experimental technique suited to a definite measurement of κ^2, the theoretical value for the so-called dynamic isotropic limit ($<\kappa^2> = 2/3$) is often used. However, the $<\kappa^2>$ uncertainty is still widely regarded as an inconvenience that may be especially important in membranes, because of their intrinsic anisotropic nature and the restricted rotational mobility experienced by fluorophores incorporated inside the bilayer. Recently, we used atomistic molecular dynamics simulations to calculate $<\kappa^2> \approx 0.87 \pm 0.06$ for homo-FRET between NBD-PC probes in fluid 16:0, 16:0 bilayers [83]. In this case, and taking into account the dependence of R_0 on κ^2 (Eq. 2), an error of ~4–5 % or ~1 Å (taking R_0(NBD-NBD) = 22–24 Å; [77]) would ensue by calculating this parameter using $<\kappa^2> = 2/3$. This relatively modest effect in ld bilayers is probably much increased in more ordered systems, such as lo- or gel-containing membranes. To this effect, and also for a more precise estimation of fluorophore transverse location, MD simulations may be an invaluable aid in design and analysis of FRET experiments. Additionally, they allow the determination of the

potential perturbation by the probes of the bilayer structure and dynamics (for a review, see Loura and Prates Ramalho [84]). After all, because the vast majority of natural lipids do not fluoresce, membrane FRET studies most often employ fluorescent probes which might behave differently in membranes when compared to the lipids they are supposed to emulate. Examples of the latter situation are the protein-lipid selectivity constants $K_s \neq 1$ recovered for probes incorporated in pure bilayers of supposedly identical (bar the fluorescent label) phospholipids, as described in Sect. 2.3. However, even in this case, adequate controls (e.g., calculating relative selectivity constants by dividing K_s for a given probe by the value recovered for the closest analog) may allow circumvention of this inconvenience.

FRET became a standard methodology under the microscope, and the most relevant application of FLIM is in energy transfer studies (FRET-FLIM). This is going to become more relevant with the foreseen instrumental developments, namely, super-resolution techniques, such as STED, now carried out up to the level of a living higher animal [6].

Acknowledgments The authors acknowledge funding by FEDER (COMPETE program) and by FCT (Fundação para a Ciência e Tecnologia); projects references: PTDC/QUI-BIQ/119494/2010, PTDC/QUI-BIQ/112067/2009, PTDC/QUI-BIQ/099947/2008, and FCOMP-01-0124-FEDER-010787 (FCT PTDC/QUI-QUI/098198/2008).

References

1. Abrams FS, London E (1993) Extension of the parallax analysis of membrane penetration depth to the polar region of model membranes: use of fluorescence quenching by a spin-label attached to the phospholipid polar headgroup. Biochemistry 32:10826–10831
2. Acasandrei MA, Dale RE, VandeVen M, Ameloot M (2006) Two-dimensional Förster resonance energy transfer (2-D FRET) and the membrane raft hypothesis. Chem Phys Lett 419:469–473
3. Almeida PFF, Vaz WLC, Thompson TE (1992) Lateral diffusion in the liquid-phases of dimyristoylphosphatidylcholine cholesterol lipid bilayers - a free-volume analysis. Biochemistry 31:6739–6747
4. Almeida PF, Pokorny A, Hinderliter A (2005) Thermodynamics of membrane domains. Biochim Biophys Acta 1720:1–13
5. Anikovsky M, Dale L, Ferguson S, Petersen N (2008) Resonance energy transfer in cells: a new look at fixation effect and receptor aggregation on cell membrane. Biophys J 95:1349–1359
6. Berning S, Willig KI, Steffens H, Dibaj P, Hell SW (2012) Nanoscopy in a living mouse brain. Science 335:551
7. Bloom M, Mouritsen OG (1995) The evolution of membranes. In: Lipowsky R, Sackmann E (eds) Handbook of biological physics, vol 1A, Structure and dynamics of membranes - from cells to vesicles. Elsevier, Amsterdam, pp 65–95
8. Bogdanov M, Dowhan W (1995) Phosphatidylethanolamine is required for in vivo function of the membrane-associated lactose permease of *Escherichia coli*. J Biol Chem 270:732–739
9. Bogdanov M, Dowhan W (1998) Phospholipid-assisted protein folding: phosphatidylethanolamine is required at a late step of the conformational maturation of the polytopic membrane protein lactose permease. EMBO J 17:5255–5264
10. Bogdanov M, Heacock PN, Dowhan W (2002) A polytopic membrane protein displays a reversible topology dependent on membrane lipid composition. EMBO J 21:2107–2116

11. Bogdanov M, Xie J, Heacock P, Dowhan W (2008) To flip or not to flip: lipid-protein charge interactions are a determinant of final membrane protein topology. J Cell Biol 182:925–935
12. Bogdanov M, Xie J, Dowhan W (2009) Lipid-protein interactions drive membrane protein topogenesis in accordance with the positive inside rule. J Biol Chem 284:9637–9641
13. Bogdanov M, Heacock P, Guan Z, Dowhan W (2010) Plasticity of lipid-protein interactions in the function and topogenesis of the membrane protein lactose permease from *Escherichia coli*. Proc Natl Acad Sci USA 107:15057–15062
14. Breitenstein D, Batenburg JJ, Hagenhoff B, Galla HJ (2006) Lipid specificity of surfactant protein B studied by time-of-flight secondary ion mass spectrometry. Biophys J 91:1347–1356
15. Brown AC, Towles KB, Wrenn SP (2007) Measuring raft size as a function of membrane composition in PC-based systems: Part I - binary systems. Langmuir 23:11180–11187
16. Brown DA, London E (2000) Structure and function of sphingolipid- and cholesterol-rich membrane rafts. J Biol Chem 275:17221–17224
17. Buboltz JT (2007) Steady-state probe-partitioning FRET: A simple and robust tool for the study of membrane phase behavior. Phys Rev E 76:021903
18. Buboltz JT, Bwalya C, Reyes S, Kamburov D (2007) Stern-Volmer modeling of steady-state Forster energy transfer between dilute, freely diffusing membrane-bound fluorophores. J Chem Phys 127:215101
19. Buboltz JT, Bwalya C, Williams K, Schutzer M (2007) High resolution mapping of phase behavior in a ternary lipid mixture: do lipid-raft phase boundaries depend on sample-prep procedure? Langmuir 23:11968–11971
20. Cabré EJ, Loura LMS, Fedorov A, Pérez-Gil J, Prieto M (2012) Topology and lipid selectivity of pulmonary surfactant protein SP-B in membranes: answers from fluorescence. Biochim Biophys Acta. doi:10.1016/j.bbamem.2012.03.008
21. Castro BM, de Almeida RF, Goormaghtigh E, Fedorov A, Prieto M (2011) Organization and dynamics of Fas transmembrane domain in raft membranes and modulation by ceramide. Biophys J 101:1632–1641
22. Chachaty C, Rainteau D, Tessier C, Quinn PJ, Wolf C (2005) Building up of the liquid-ordered phase formed by sphingomyelin and cholesterol. Biophys J 88:4032–4044
23. Chattopadhyay A (1990) Chemistry and biology of N-(7-nitrobenz-2-oxa-1,3-diazol-4-yl)-labeled lipids: fluorescent probes of biological and model membranes. Chem Phys Lipids 53:1–15
24. Chen CC, Wilson TH (1984) The phospholipid requirement for activity of the lactose carrier of *Escherichia coli*. J Biol Chem 259:10150–10158
25. Chiantia S, Kahya N, Schwille P (2007) Raft domain reorganization driven by short- and long-chain ceramide: a combined AFM and FCS study. Langmuir 23:7659–7665
26. Clements JA (1977) Functions of the alveolar lining. Am Rev Respir Dis 115:67–71
27. Coutinho A, Loura LMS, Fedorov A, Prieto M (2008) Pinched multilamellar structure of aggregates of lysozyme and phosphatidylserine-containing membranes revealed by FRET. Biophys J 95:4726–4736
28. Cruz A, Casals C, Plasencia I, Marsh D, Pérez-Gil J (1998) Depth profiles of pulmonary surfactant protein B in phosphatidylcholine bilayers, studied by fluorescence and electron spin resonance spectroscopy. Biochemistry 37:9488–9496
29. Cruz A, Marsh D, Pérez-Gil J (1998) Rotational dynamics of spin-labelled surfactant-associated proteins SP-B and SP-C in dipalmitoylphosphatidylcholine and dipalmitoylphosphatidylglycerol bilayers. Biochim Biophys Acta 1415:125–134
30. Czech MP (2000) PIP2 and PIP3: complex roles at the cell surface. Cell 100:603–606
31. Davenport L (1997) Fluorescence probes for studying membrane heterogeneity. Meth Enzymol 278:487–512
32. de Almeida RFM, Loura LMS, Fedorov A, Prieto M (2002) Nonequilibrium phenomena in the phase separation of a two-component lipid bilayer. Biophys J 82:823–834

33. de Almeida RFM, Fedorov A, Prieto M (2003) Sphingomyelin/Phosphatidylcholine/Cholesterol phase diagram: boundaries and composition of lipid rafts. Biophys J 85:2406–2416
34. de Almeida RFM, Loura LMS, Prieto M, Watts A, Fedorov A, Barrantes FJ (2004) Cholesterol modulates the organization of the γM4 transmembrane domain of the muscle nicotinic acetylcholine receptor. Biophys J 86:2261–2272
35. de Almeida RFM, Loura LMS, Fedorov A, Prieto M (2005) Lipid rafts have different sizes depending on membrane composition: a time-resolved fluorescence resonance energy transfer study. J Mol Biol 346:1109–1120
36. de Almeida RFM, Borst J, Fedorov A, Prieto M, Visser AJWG (2007) Complexity of lipid domains and rafts in giant unilamellar vesicles revealed by combining imaging and microscopic and macroscopic time-resolved fluorescence. Biophys J 93:539–553
37. de Almeida RF, Loura LMS, Prieto M (2009) Membrane lipid domains and rafts: current applications of fluorescence lifetime spectroscopy and imaging. Chem Phys Lipids 157:61–77
38. Dickenson NE, Armendariz KP, Huckabay HA, Livanec PW, Dunn RC (2010) Near-field scanning optical microscopy: a tool for nanometric exploration of biological membranes. Anal Bioanal Chem 396:31–43
39. Dico AS, Hancock J, Morrow MR, Stewart J, Harris S, Keough KM (1997) Pulmonary surfactant protein SP-B interacts similarly with dipalmitoylphosphatidylglycerol and dipalmitoylphosphatidylcholine in phosphatidylcholine/phosphatidylglycerol mixtures. Biochemistry 36:4172–4177
40. Dowhan W (1997) Molecular basis for membrane phospholipid diversity: why are there so many lipids? Annu Rev Biochem 66:199–232
41. Fernandes F, Loura LMS, Prieto M, Koehorst R, Spruijt R, Hemminga MA (2003) Dependence of M13 major coat protein oligomerization and lateral segregation on bilayer composition. Biophys J 85:2430–2441
42. Fernandes F, Loura LM, Koehorst R, Spruijt RB, Hemminga MA, Fedorov A, Prieto M (2004) Quantification of protein-lipid selectivity using FRET: application to the M13 major coat protein. Biophys J 87:344–352
43. Fernandes F, Loura LMS, Fedorov A, Prieto M (2006) Absence of clustering of phosphatidylinositol-(4,5)-bisphosphate in fluid phosphatidylcholine. J Lipid Res 47:1521–1525
44. Förster T (1949)) Experimentelle und theoretische Untersuchung des Zwischenmolekularen übergangs von Elektrinenanregungsenergie. Z Naturforsch 4a:321–327
45. Frazier ML, Wright JR, Pokorny A, Almeida PF (2007) Investigation of domain formation in sphingomyelin/cholesterol/POPC mixtures by fluorescence resonance energy transfer and Monte Carlo simulations. Biophys J 92:2422–2433
46. Fung BK, Stryer L (1978) Surface density determination in membranes by fluorescence energy transfer. Biochemistry 17:5241–5248
47. Goswami D, Gowrishankar K, Bilgrami S, Ghosh S, Raghupathy R, Chadda R, Vishwakarma R, Rao M, Mayor S (2008) Nanoclusters of GPI-anchored proteins are formed by cortical actin-driven activity. Cell 135:1085–1097
48. Heberle FA, Wu J, Goh SL, Petruzielo RS, Feigenson GW (2010) Comparison of three ternary lipid bilayer mixtures: FRET and ESR reveal nanodomains. Biophys J 99:3309–3318
49. Hemminga MA, Sanders JC, Spruijt RB (1992) Spectroscopy of lipid-protein interactions: structural aspects of two different forms of the coat protein of bacteriophage M13 incorporated in model membranes. Prog Lipid Res 31:301–333
50. Hofman EG, Ruonala MO, Bader AN, van den Heuvel D, Voortman J, Roovers RC, Verkleij AJ, Gerritsen HC, van Bergen en Henegouwen PMP (2008) EGF induces coalescence of different lipid rafts. J Cell Sci 121:2519–2528
51. Holt A, de Almeida RFM, Nyholm TK, Loura LMS, Daily AE, Staffhorst RW, Rijkers DT, Koeppe RE 2nd, Prieto M, Killian JA (2008) Is there a preferential interaction between cholesterol and tryptophan residues in membrane proteins? Biochemistry 47:2638–2649

52. Goñi FM, Alonso A, Bagatolli LA, Brown RE, Marsh D, Prieto M, Thewalt JL (2008) Phase diagrams of lipid mixtures relevant to the study of membrane rafts. Biochim Biophys Acta 1781:665–684
53. Grecco HE, Roda-Navarro P, Verveer PJ (2009) Global analysis of time correlated single photon counting FRET-FLIM data. Opt Express 17:6493–6508
54. Guan L, Smirnova IN, Verner G, Nagamori S, Kaback HR (2006) Manipulating phospholipids for crystallization of a membrane transport protein. Proc Natl Acad Sci USA 103:1723–1726
55. Gutberlet T, Dietrich U, Bradaczek H, Pohlentz G, Leopold K, Fischer W (2000) Cardiolipin, alpha-D-glucopyranosyl, and L-lysylcardiolipin from gram-positive bacteria: FAB MS, monofilm and X-ray powder diffraction studies. Biochim Biophys Acta 1463:307–322
56. Herreros J, Ng T, Schiavo G (2001) Lipid rafts act as specialized domains for tetanus toxin binding and internalization into neurons. Mol Biol Cell 12:2947–2960
57. Hughes WE, Larijani B, Parker PJ (2002) Detecting protein-phospholipid interactions. J Biol Chem 277:22974–22979
58. Ipsen JH, Karlström G, Mouritsen OG, Wennerström H, Zuckermann MJ (1987) Phase equilibria in the phosphatidylcholine-cholesterol system. Biochim Biophys Acta 905:162–172
59. Jacobson K, Mouritsen OG, Anderson RG (2007) Lipid rafts: at a crossroad between cell biology and physics. Nat Cell Biol 9:7–14
60. Jares-Erijman EA, Jovin TM (2006) Imaging molecular interactions in living cells by FRET microscopy. Curr Opin Chem Biol 10:409–416
61. Johansson J, Curstedt T (1997) Molecular structures and interactions of pulmonary surfactant components. Eur J Biochem 244:675–693
62. Johansson J, Curstedt T, Jornvall H (1991) Surfactant protein B: disulfide bridges, structural properties, and Kringle similarities. Biochemistry 30:6917–6921
63. Jørgensen K, Klinger A, Biltonen RL (2000) Nonequilibrium lipid domain growth in the gel-fluid two phase region of a $DC_{16}PC$-$DC_{22}PC$ lipid mixture investigated by Monte-Carlo computer simulation, FT-IR and fluorescence spectroscopy. J Phys Chem 104:11763–11773
64. Karmakar S, Raghunathan VA, Mayor S (2005) Phase behaviour of dipalmitoylphospatidylcholine (DPPC)-cholesterol membranes. J Phys Condens Matter 17:S1177–S1182
65. Kenworthy AK, Edidin M (1998) Distribution of a glycosylphosphatidylinositol-anchored protein at the apical surface of MDCK cells examined at a resolution of <100 Å using imaging fluorescence resonance energy transfer. J Cell Biol 142:69–84
66. Kiskowski MA, Kenworthy AK (2007) In silico characterization of resonance energy transfer for disk-shaped membrane domains. Biophys J 92:3040–3051
67. Koehorst RB, Spruijt RB, Vergeldt FJ, Hemminga MA (2004) Lipid bilayer topology of the transmembrane alpha-helix of M13 Major coat protein and bilayer polarity profile by site-directed fluorescence spectroscopy. Biophys J 87:1445–1455
68. Kusumi A, Nakada C, Ritchie K, Murase K, Suzuki K, Murakoshi H, Kasai RS, Kondo J, Fujiwara T (2005) Paradigm shift of the plasma membrane concept from the two-dimensional continuum fluid to the partitioned fluid: high-speed single-molecule tracking of membrane molecules. Annu Rev Biophys Biomol Struct 34:351–378
69. Lantzsch G, Binder H, Heerklotz H (1994) Surface area per molecule in lipid/$C12E_n$ membranes as seen by fluorescence resonance energy transfer. J Fluoresc 4:339–343
70. Lakowicz JR (2006) Principles of fluorescence spectroscopy. Kluwer Academic/Plenum, New York
71. Lee AG (2003) Lipid-protein interactions in biological membranes: a structural perspective. Biochim Biophys Acta 1612:1–40
72. Lentz BR, Barrow DA, Hoechli M (1980) Cholesterol-phosphatidylcholine interactions in multilamellar vesicles. Biochemistry 19:1943–1954

73. Li M, Reddy LG, Bennett R, Silva ND Jr, Jones LR, Thomas DD (1999) A fluorescence energy transfer method for analyzing protein oligomeric structure: application to phospholamban. Biophys J 76:2587–2599
74. Loura LMS, Prieto M (2000) Resonance energy transfer in heterogeneous planar and bilayer systems: theory and simulation. J Phys Chem B 104:6911–6919
75. Loura LM, Ramalho JP (2007) Location and dynamics of acyl chain NBD-labeled phosphatidylcholine (NBD-PC) in DPPC bilayers. A molecular dynamics and time-resolved fluorescence anisotropy study. Biochim Biophys Acta 1768:467–478
76. Loura LMS, Fedorov A, Prieto M (1996) Resonance energy transfer in a model system of membranes: application to gel and liquid crystalline phases. Biophys J 71:1823–1836
77. Loura LMS, Fedorov A, Prieto M (2000) Membrane probe distribution heterogeneity: a resonance energy transfer study. J Phys Chem B 104:6920–6931
78. Loura LMS, Fedorov A, Prieto M (2000) Partition of membrane probes in a gel/fluid two-component lipid system: a fluorescence resonance energy transfer study. Biochim Biophys Acta 1467:101–112
79. Loura LMS, Fedorov A, Prieto M (2001) Fluid-fluid membrane microheterogeneity: a fluorescence resonance energy transfer study. Biophys J 80:776–788
80. Loura LMS, Coutinho A, Silva A, Fedorov A, Prieto M (2006) Structural effects of a basic peptide on the organization of dipalmitoylphosphatidylcholine/dipalmitoylphosphatidylserine membranes: a fluorescent resonance energy transfer study. J Phys Chem B 110:8130–8141
81. Loura LMS, Fernandes F, Prieto M (2010) Membrane microheterogeneity: Förster resonance energy transfer characterization of lateral membrane domains. Eur Biophys J 39:589–607
82. Loura LMS, Prieto M, Fernandes F (2010) Quantification of protein-lipid selectivity using FRET. Eur Biophys J 39:565–578
83. Loura LMS, Palace Carvalho AJ, Prates Ramalho JP (2010) Direct calculation of Förster orientation factor of membrane probes by molecular simulation. J Mol Struct THEOCHEM 946:107–112
84. Loura LMS, Prates Ramalho JP (2011) Recent developments in molecular dynamics simulations of fluorescent membrane probes. Molecules 16:5437–5452
85. Mabrey S, Sturtevant JM (1976) Investigation of phase transitions of lipids and lipid mixtures by sensitivity differential scanning calorimetry. Proc Natl Acad Sci U S A 73:3862–3866
86. Marsh D (1990) Handbook of Lipid Bilayers. CRC Press, Boca Raton
87. Marsh D (2010) Liquid-ordered phases induced by cholesterol: a compendium of binary phase diagrams. Biochim Biophys Acta 1798:688–699
88. Marsh D, Horváth LI (1998) Structure, dynamics and composition of the lipid-protein interface. Perspectives from spin-labelling. Biochim Biophys Acta 1376:267–296
89. Mateo CR, Acuna AU, Brochon J-C (1995) Liquid-crystalline phases of cholesterol lipid bilayers as revealed by the fluorescence of *trans*-parinaric acid. Biophys J 68:978–987
90. Mayor S, Rao M (2004) Rafts: scale-dependent, active lipid organization at the cell surface. Traffic 5:231–240
91. Mazères S, Schram V, Tocanne JF, Lopez A (1996) 7-nitrobenz-2-oxa-1,3-diazole-4-yl-labeled phospholipids in lipid membranes: differences in fluorescence behavior. Biophys J 71:327–335
92. McMullen TP, McElhaney RN (1995) New aspects of the interaction of cholesterol with dipalmitoylphosphatidylcholine bilayers as revealed by high-sensitivity differential scanning calorimetry. Biochim Biophys Acta 1234:90–98
93. Meyer BH, Segura J-M, Martinez KL, Hovius R, George N, Johnsson K, Vogel H (2006) FRET imaging reveals that functional neurokinin-1 receptors are monomeric and reside in membrane microdomains of live cells. Proc Natl Acad Sci USA 103:2138–2143
94. Morrow MR, Pérez-Gil J, Simatos G, Boland C, Stewart J, Absolom D, Sarin V, Keough KM (1993 Apr 27) Pulmonary surfactant-associated protein SP-B has little effect on acyl chains in dipalmitoylphosphatidylcholine dispersions. Biochemistry 32(16):4397–402

95. Mouritsen OG, Bloom M (1984) Mattress model of lipid-protein interactions in membranes. Biophys J 46:141–153
96. Needham D, Nunn RS (1990) Elastic deformation and failure of lipid bilayer membranes containing cholesterol. Biophys J 58:997–1009
97. Notter RH, Finkelstein JN (1984) Pulmonary surfactant: an interdisciplinary approach. J Appl Physiol 57:1613–1624
98. O'Keefe AH, East JM, Lee AG (2000) Selectivity in lipid binding to the bacterial outer membrane protein OmpF. Biophys J 79:2066–2074
99. Oosterlaken-Dijksterhuis MA, Haagsman HP, van Golde LM, Demel RA (1991) Characterization of lipid insertion into monomolecular layers mediated by lung surfactant proteins SP-B and SP-C. Biochemistry 30:10965–10971
100. Oosterlaken-Dijksterhuis MA, van Eijk M, van Golde LM, Haagsman HP (1992) Lipid mixing is mediated by the hydrophobic surfactant protein SP-B but not by SP-C. Biochim Biophys Acta 1110:45–50
101. Owen DM, Neil MAA, French PMW, Magee AI (2007) Optical techniques for imaging membrane lipid microdomains in living cells. Sem Cell Develop Biol 18:591–598
102. Owen DM, Gaus K, Magee AI, Cebecauer M (2010) Dynamic organization of lymphocyte plasma membrane: lessons from advanced imaging methods. Immunology 131:1–8
103. Padilla-Parra S, Auduge N, Coppey-Moisan M, Tramier M (2008) Quantitative FRET analysis by fast acquisition time domain FLIM at high spatial resolution in living cells. Biophys J 95:2976–2988
104. Peelen SJ, Sanders JC, Hemminga MA, Marsh D (1992) Stoichiometry, selectivity, and exchange dynamics of lipid-protein interaction with bacteriophage M13 coat protein studied by spin label electron spin resonance. Effects of protein secondary structure. Biochemistry 31:2670–2677
105. Pérez-Gil J (2001) Lipid-protein interactions of hydrophobic proteins SP-B and SP-C in lung surfactant assembly and dynamics. Pediatr Pathol Mol Med 20:445–469
106. Pérez-Gil J, Keough KM (1998) Interfacial properties of surfactant proteins. Biochim Biophys Acta 1408:203–217
107. Pérez-Gil J, Casals C, Marsh D (1995) Interactions of hydrophobic lung surfactant proteins SP-B and SP-C with dipalmitoylphosphatidylcholine and dipalmitoylphosphatidylglycerol bilayers studied by electron spin resonance spectroscopy. Biochemistry 34:3964–3971
108. Picas L, Suárez-Germà C, Montero MT, Vázquez-Ibar JL, Hernández-Borrell J, Prieto M, Loura LM (2010) Lactose permease lipid selectivity using Förster resonance energy transfer. Bio-chim Biophys Acta 1798:1707–1713
109. Pluschke G, Hirota Y, Overath P (1978) Function of phospholipids in *Escherichia coli*. Charac-terization of a mutant deficient in cardiolipin synthesis. J Biol Chem 253:5048–5055
110. Poulain FR, Allen L, Williams MC, Hamilton RL, Hawgood S (1992) Effects of surfactant apolipoproteins on liposome structure: implications for tubular myelin formation. Am J Physiol 262:L730–L739
111. Powl AM, East JM, Lee AG (2003) Lipid-protein interactions studied by introduction of a tryp-tophan residue: the mechanosensitive channel MscL. Biochemistry 42:14306–14317
112. Rand RP, Parsegian VA (1989) Hydration forces between phospholipid-bilayers. Biochim Biophys Acta 988:351–376
113. Rao M, Mayor S (2005) Use of Förster's resonance energy transfer microscopy to study lipid rafts. Biochim Biophys Acta 1746:221–233
114. Ryan MA, Qi X, Serrano AG, Ikegami M, Perez-Gil J, Johansson J, Weaver TE (2005) Mapping and analysis of the lytic and fusogenic domains of surfactant protein B. Biochemistry 44:861–872
115. Šachl R, Humpolíčková J, Stefl M, Johansson LB, Hof M (2011) Limitations of electronic energy transfer in the determination of lipid nanodomain sizes. Biophys J 101:L60–L62
116. Seifert M, Breitenstein D, Klenz U, Meyer MC, Galla HJ (2007) Solubility versus electrostatics: what determines lipid/protein interaction in lung surfactant. Biophys J 93:1192–1203

117. Sharma P, Varma R, Sarasij RC, Gousset K, Ira RC, Krishnamoorthy G, Rao M, Mayor S (2004) Nanoscale organization of multiple GPI-anchored proteins in living cell membranes. Cell 116:577–589
118. Shiffer K, Hawgood S, Haagsman HP, Benson B, Clements JA, Goerke J (1993) Lung surfactant proteins, SP-B and SP-C, alter the thermodynamic properties of phospholipid membranes: a differential calorimetry study. Biochemistry 32:590–597
119. Silva L, de Almeida RF, Fedorov A, Matos AP, Prieto M (2006) Ceramide-platform formation and -induced biophysical changes in a fluid phospholipid membrane. Mol Membr Biol 23:137–148
120. Silva LC, de Almeida RF, Castro BM, Fedorov A, Prieto M (2007) Ceramide-domain formation and collapse in lipid rafts: membrane reorganization by an apoptotic lipid. Biophys J 92:502–516
121. Simons K, Vaz WL (2004) Model systems, lipid rafts, and cell membranes. Annu Rev Biophys Biomol Struct 33:269–295
122. Singer SJ, Nicolson GL (1972) The fluid mosaic model of the structure of cell membranes. Science 175:720–731
123. Soubias O, Teague WE Jr, Hines KG, Mitchell DC, Gawrisch K (2010) Contribution of membrane elastic energy to rhodopsin function. Biophys J 99:817–824
124. Spruijt RB, Wolfs CJ, Verver JW, Hemminga MA (1996) Accessibility and environment probing using cysteine residues introduced along the putative transmembrane domain of the major coat protein of bacteriophage M13. Biochemistry 35:10383–10391
125. Stöckl MT, Herrmann A (2010) Detection of lipid domains in model and cell membranes by fluorescence lifetime imaging microscopy. Biochim Biophys Acta 1798:1444–1456
126. Stopar D, Jansen KA, Páli T, Marsh D, Hemminga MA (1997) Membrane location of spin-labeled M13 major coat protein mutants determined by paramagnetic relaxation agents. Biochemistry 36:8261–8268
127. Stopar D, Spruijt RB, Wolfs CJ, Hemminga MA (2003) Protein-lipid interactions of bacteriophage M13 major coat protein. Biochim Biophys Acta 1611:5–15
128. Stryer L (1978) Fluorescence energy transfer as a spectroscopic ruler. Annu Rev Biochem 47:819–846
129. Suárez-Germà C, Loura LMS, Prieto M, Domènech O, Montero MT, Rodríguez-Banqueri A, Vázquez-Ibar JL, Hernández-Borrell J (2012) Membrane protein-lipid selectivity: enhancing sensitivity for modeling FRET data. J Phys Chem B 116:2438–2445
130. Tahara Y, Murata M, Ohnishi S, Fujiyoshi Y, Kikuchi M, Yamamoto Y (1992) Functional signal peptide reduces bilayer thickness of phosphatidylcholine liposomes. Biochemistry 31:8747–8754
131. Towles KB, Dan N (2007) Determination of membrane domain size by fluorescence resonance energy transfer: effects of domain polydispersity and packing. Langmuir 23:4737–4739
132. Towles KB, Brown AC, Wrenn SP, Dan N (2007) Effect of membrane microheterogeneity and domain size on fluorescence resonance energy transfer. Biophys J 93:655–667
133. Vandenbussche G, Clercx A, Clercx M, Curstedt T, Johansson J, Jörnvall H, Ruysschaert JM (1992) Secondary structure and orientation of the surfactant protein SP-B in a lipid environment. A Fourier transform infrared spectroscopy study. Biochemistry 31:9169–9176
134. Van Der Meer B, Coker G 3rd, Chen S-YS (1994) Resonance energy transfer: theory and data. VCH Publishers, New York
135. Varma R, Mayor S (1998) GPI-anchored proteins are organized in submicron domains at the cell surface. Nature 394:798–801
136. Veatch SL, Keller SL (2003) Separation of liquid phases in giant vesicles of ternary mixtures of phospholipids and cholesterol. Biophys J 85:3074–3083
137. Veatch SL, Keller SL (2005) Miscibility phase diagrams of giant vesicles containing sphingomyelin. Phys Rev Lett 94:148101–148104
138. Veatch SL, Keller SL, Gawrisch K (2007) Critical fluctuations in domain-forming lipid mixtures. Proc Natl Acad Sci USA 104:17650–17655

139. Veatch SL, Polozov IV, Gawrisch K, Keller SL (2004) Liquid domains in vesicles investigated by NMR and fluorescence microscopy. Biophys J 86:2910–2922
140. Vist MR, Davis JH (1990) Phase equilibria of cholesterol/dipalmitoylphosphatidylcholine mixtures: 2 H nuclear magnetic resonance and differential scanning calorimetry. Biochemistry 29:451–464
141. Von Arnim CAF, Kinoshita A, Peltan ID, Tangredi MM, Herl L, Lee BM, Spoelgen R, Hshieh TT, Ranganathan S, Battey FD, Liu CX, Bacskai BJ, Sever S, Irizarry MC, Strickland DK, Hyman BT (2005) The low density lipoprotein receptor-related protein (LRP) is a novel beta-secretase (BACE1) substrate. J Biol Chem 280:17777–17785
142. Wang X, Bogdanov M, Dowhan W (2002) Topology of polytopic membrane protein subdomains is dictated by membrane phospholipid composition. EMBO J 21:5673–5681
143. Wikström M, Kelly AA, Georgiev A, Eriksson HM, Klement MR, Bogdanov M, Dowhan W, Wieslander A (2009) Lipid-engineered *Escherichia coli* membranes reveal critical lipid headgroup size for protein function. J Biol Chem 284:954–965
144. Williamson IM, Alvis SJ, East JM, Lee AG (2002) Interactions of phospholipids with the potassium channel KcsA. Biophys J 83:2026–2038
145. Wolber PK, Hudson BS (1979) An analytical solution to the Förster energy transfer problem in two dimensions. Biophys J 28:197–210
146. Wu SH, McConnell HM (1975) Phase separations in phospholipid membranes. Biochemistry 14:847–854
147. Zaltash S, Palmblad M, Curstedt T, Johansson J, Persson B (2000) Pulmonary surfactant protein B: a structural model and a functional analogue. Biochim Biophys Acta 1466:179–186
148. Edidin M (2003) Lipids on the frontier: a century of cell-membrane bilayers. Nat Rev Mol Cell Biol 4:414–418
149. London E, Brown DA (2000) Insolubility of lipids in triton X-100: physical origin and relationship to sphingolipid/cholesterol membrane domains (rafts). Biochim Biophys Acta 1508:182–195
150. Sanders JC, Ottaviani MF, van Hoek A, Visser AJ, Hemminga MA (1992) A small protein in model membranes: a time-resolved fluorescence and ESR study on the interaction of M13 coat protein with lipid bilayers. Eur Biophys J 21:305–311